




Article

Sit4 Genetically Interacts with Vps27 to Regulate Mitochondrial Function and Lifespan in *Saccharomyces cerevisiae*

Telma S. Martins^{1,2,3}, Miguel Correia^{1,2}, Denise Pinheiro^{1,2}, Carolina Lemos^{1,2,3}, Marta Vaz Mendes^{1,2} , Clara Pereira^{1,2,*}  and Vítor Costa^{1,2,3,*} 

¹ i3S—Instituto de Investigação e Inovação em Saúde, Universidade do Porto, 4200-135 Porto, Portugal; telma.martins@ibmc.up.pt (T.S.M.); miguelc@i3s.up.pt (M.C.); dpinheiro@i3s.up.pt (D.P.); cclemos@ibmc.up.pt (C.L.); mvm@ibmc.up.pt (M.V.M.)

² IBMC—Instituto de Biologia Molecular e Celular, Universidade do Porto, 4200-135 Porto, Portugal

³ ICBAS—Instituto de Ciências Biomédicas Abel Salazar, Universidade do Porto, 4050-313 Porto, Portugal

* Correspondence: clara.pereira@ibmc.up.pt (C.P.); vcosta@ibmc.up.pt (V.C.)

Abstract: The Sit4 protein phosphatase plays a key role in orchestrating various cellular processes essential for maintaining cell viability during aging. We have previously shown that *SIT4* deletion promotes vacuolar acidification, mitochondrial derepression, and oxidative stress resistance, increasing yeast chronological lifespan. In this study, we performed a proteomic analysis of isolated vacuoles and yeast genetic interaction analysis to unravel how Sit4 influences vacuolar and mitochondrial function. By employing high-resolution mass spectrometry, we show that *sit4Δ* vacuolar membranes were enriched in Vps27 and Hse1, two proteins that are part of the endosomal sorting complex required for transport-0. In addition, *SIT4* exhibited a negative genetic interaction with *VPS27*, as *sit4Δvps27Δ* double mutants had a shortened lifespan compared to *sit4Δ* and *vps27Δ* single mutants. Our results also show that Vps27 did not increase *sit4Δ* lifespan by improving protein trafficking or vacuolar sorting pathways. However, Vps27 was critical for iron homeostasis and mitochondrial function in *sit4Δ* cells, as *sit4Δvps27Δ* double mutants exhibited high iron levels and impaired mitochondrial respiration. These findings show, for the first time, cross-talk between Sit4 and Vps27, providing new insights into the mechanisms governing chronological lifespan.

Keywords: Sit4; Vps27; vacuolar trafficking; mitochondria; iron; chronological aging



Citation: Martins, T.S.; Correia, M.; Pinheiro, D.; Lemos, C.; Mendes, M.V.; Pereira, C.; Costa, V. Sit4 Genetically Interacts with Vps27 to Regulate Mitochondrial Function and Lifespan in *Saccharomyces cerevisiae*. *Cells* **2024**, *13*, 655. <https://doi.org/10.3390/cells13080655>

Academic Editor: Christoph Englert

Received: 6 January 2024

Revised: 27 March 2024

Accepted: 6 April 2024

Published: 9 April 2024



Copyright: © 2024 by the authors. Licensee MDPI, Basel, Switzerland. This article is an open access article distributed under the terms and conditions of the Creative Commons Attribution (CC BY) license (<https://creativecommons.org/licenses/by/4.0/>).

1. Introduction

Lysosomes and lysosome-like vacuoles in yeast serve as pivotal hubs for maintaining cellular homeostasis, metabolism, and lifespan. These organelles are enriched in carrier proteins and hydrolases, such as proteases, glycosidases, lipases, nucleases, phosphatases, and sulfatases. The concentration of these hydrolases and the vacuolar H⁺-ATPase-dependent maintenance of an acidic pH render lysosomes a major catabolic center [1–5]. Notably, lysosomal dysfunction is a hallmark of aging common to several age-related diseases, including cancer and neurodegenerative and metabolic disorders [1,6]. The decline in lysosomal function during aging has been linked to the dysregulation of nutrient signaling pathways, an increase in lysosomal pH, and a decrease in autophagy [1,7–11]. Notably, lifespan extension by dietary restriction involves the modulation of nutrient signaling pathways, which in turn depend at least in part on lysosome function in several organisms [7,12–18].

Lysosomes degrade both intracellular and exogenous components, from macromolecules to organelles, such as mitochondria, peroxisomes, or lipid droplets, and even surface receptors and pathogens. The major pathways of substrate delivery to lysosomes are autophagy and the endocytic pathway [2,19]. For example, during macroautophagy (hereafter named autophagy), a double membrane is formed around cytoplasmic material targeted for degradation, leading to the generation of autophagosomes that ultimately merge with lysosomes [20,21]. Conversely, mitophagy allows the selective clearance of mitochondria [22]. Autophagy is

highly conserved during evolution and serves critical roles in ensuring cell survival [23,24]. It maintains protein and organelle quality control by removing damaged material that is generated under stress conditions and during aging or diseases. In addition, it allows cells to survive under nutrient deprivation by recycling macromolecules, to provide amino acids, sugars, fatty acids, nucleotides, and other nutrients. The endocytic pathway plays a vital role in regulating cellular functions and immune responses by delivering extracellular and cell surface cargos to lysosomes via endocytosis [25,26]. Internalized proteins localized at early endosomes undergo sorting, being either targeted for degradation in lysosomes or recycled to other compartments (e.g., the Golgi apparatus and the plasma membrane). Proteins destined for degradation are ubiquitinated, allowing their recognition by the endosomal sorting complex required for transport (ESCRT), which facilitates its sorting via the multivesicular body (MVB) pathway to the lysosome. Conversely, proteins that are not ubiquitinated follow the recycling pathway [27,28].

Trafficking pathways play a vital role in the function and biogenesis of vacuoles. In eukaryotic cells, organellar proteins are produced in the ER, moved to the Golgi apparatus, and subsequently sorted into their cellular compartments. In yeast, proteins destined for the vacuole can follow three routes: the carboxypeptidase Y (CPY) pathway (indirectly, through late endosomes/MVB), the alkaline phosphatase (ALP/AP-3) pathway [26,29], or the cytoplasm to vacuole targeting (Cvt) pathway, which uses much of the autophagic machinery to transport hydrolases, such as α -mannosidase (Ams1) and aminopeptidase I (Ape1), from the cytoplasm to the vacuole [30].

Apart from their essential function in degradation, lysosomes also serve as storage site for metabolites derived from the diet (e.g., amino acids, sugars, lipids, nucleotides, and ions) and play a central role in regulating nutrient sensing and signaling pathways [4,5]. For instance, vacuolar iron storage is particularly important to prevent oxidative stress, as it is a redox-active metal [31].

Targeting lysosomes to optimize their function is emerging as a means to promote a healthier lifespan [1,3,6,7,11]. This promising strategy requires a deeper comprehension of the molecular cues driving the decline in lysosomal function with age and its improvement under lifespan extension conditions. We have previously shown that *SIT4* deletion increases yeast chronological lifespan (CLS) by promoting vacuolar acidification as well as mitochondrial derepression and oxidative stress resistance [32–35]. Sit4 is a PP2A-like Ser/Thr protein phosphatase, a homologue of the mammalian protein phosphatase 6 (PP6) [36], which is also involved in the regulation of the cell cycle and budding [37,38], cell wall integrity, actin cytoskeleton organization and ribosomal gene expression mediated by Pkc1 function [39], nutrient signaling [40,41], carbohydrate and lipid metabolism [42,43], pH and monovalent ion homeostasis [44], and ER-to-Golgi trafficking [45]. Sit4 acts as the catalytic subunit of several protein complexes, formed by its association with distinct regulatory subunits, explaining its role across a broad array of cellular functions. For instance, Sit4-associated proteins (SAPs), namely Sap4, Sap155, Sap185, or Sap190, bind Sit4 independently to positively regulate cell cycle progression at the G1 phase [46]. Sit4 can also form a ceramide-activated protein phosphatase complex by interacting with regulatory subunits Tpd3 and Cdc55 [47]. In addition, Sit4 interacts with and is inhibited by Tap42 in response to nutrient signals through TORC1 [40]. The dissociation of the Tap42-Sit4 complex results in Sit4 activation and dephosphorylation of the GATA-binding transcription factor Gln3, which is then translocated into the nucleus where it activates the nitrogen catabolite repression pathway [48].

In this study, we assessed how Sit4 deficiency impacts vacuoles by performing a proteomic analysis of vacuolar membranes from wild-type and *sit4* Δ cells and investigated the role of Vps27 in regulating *sit4* Δ CLS. Our findings reveal that Vps27 is enriched in the vacuolar membranes of *sit4* Δ cells and is crucial for lifespan extension by modulating mitochondrial function.

2. Materials and Methods

2.1. Yeast Strains and Growth Conditions

The *S. cerevisiae* strains utilized in this study are detailed in Table 1. Yeast cells were cultured aerobically at 26 °C on an orbital shaker set at 140 rpm, maintaining a flask volume to medium volume of 5:1. Synthetic complete (SC) medium was used as a growth medium, comprising drop-out, 2% (*w/v*) glucose (Thermo Fisher Scientific, Waltham, MA, USA), and 0.67% (*w/v*) yeast nitrogen base without amino acids (BD BioSciences, San Jose, CA, USA), supplemented with the required amino acids and nucleotides. For BY4741 strains, SC medium was supplemented with histidine (0.008% (*w/v*), Sigma Aldrich, St. Louis, MO, USA), methionine (0.038% (*w/v*), Sigma Aldrich, St. Louis, MO, USA), leucine (0.04% (*w/v*), Sigma Aldrich, St. Louis, MO, USA), and uracil (0.008% (*w/v*), Sigma Aldrich, St. Louis, MO, USA). For BY4742 strains, SC medium was supplemented with histidine (0.008% (*w/v*), Sigma Aldrich, St. Louis, MO, USA), lysine (0.008% (*w/v*), Sigma Aldrich, St. Louis, MO, USA), leucine (0.04% (*w/v*), Sigma Aldrich, St. Louis, MO, USA), and uracil (0.008% (*w/v*), Sigma Aldrich, St. Louis, MO, USA). To assess Mup1-GFP levels in response to methionine, BY4742 cells were cultured in minimal medium (MM), containing 2% (*w/v*) glucose (Thermo Fisher Scientific, Waltham, MA, USA) and 0.67% (*w/v*) yeast nitrogen base without amino acids (BD BioSciences, San Jose, CA, USA), supplemented with amino acids or nucleotides [0.008% (*w/v*) histidine (Sigma Aldrich, St. Louis, MO, USA), 0.008% (*w/v*) lysine (Sigma Aldrich, St. Louis, MO, USA), 0.04% (*w/v*) leucine (Sigma Aldrich, St. Louis, MO, USA), and 0.008% (*w/v*) uracil (Sigma Aldrich, St. Louis, MO, USA)]. Furthermore, 38 mg L⁻¹ of L-methionine (Thermo Fisher Scientific, Waltham, MA, USA) was added to cell cultures.

Table 1. *Saccharomyces cerevisiae* strains used in this study.

Strain	Genotype	Source
BY4741 ^{b,e,f}	Mata, <i>his3Δ1</i> , <i>leu2Δ0</i> , <i>met15Δ0</i> , <i>ura3Δ0</i>	EUROSCARF
<i>sit4Δ</i> ^{b,e,f}	BY4741 <i>sit4::MXHIS3</i>	[34]
<i>vps27Δ</i> ^{a,b,e,f}	BY4741 <i>vps27::KanMX4</i>	This study
<i>sit4Δvps27Δ</i> ^{a,b,e,f}	BY4741 <i>sit4::MXHIS3 vps27::KanMX4</i>	This study
<i>pep4Δ</i>	BY4741 <i>pep4::KanMX4</i>	EUROSCARF
<i>pho8Δ</i> ^c	BY4741 <i>pho8::HPH</i>	[49]
<i>sit4Δpho8Δ</i> ^c	BY4741 <i>sit4::KanMX4 pho8::HPH</i>	[49]
<i>vps27Δpho8Δ</i> ^c	BY4741 <i>vps27::MXHIS3 pho8::HPH</i>	This study
<i>sit4Δvps27Δpho8Δ</i> ^c	BY4741 <i>sit4::KanMX4 vps27::MXHIS3 pho8::HPH</i>	This study
BY4742 ^d	Mata <i>his3Δ1</i> , <i>leu2Δ0</i> , <i>lys2Δ0</i> , <i>ura3Δ0</i>	EUROSCARF
<i>sit4Δ</i> ^d	BY4742 <i>sit4::KanMX4</i>	EUROSCARF
<i>vps27Δ</i> ^d	BY4742 <i>vps27::MXHIS3</i>	This study
<i>sit4Δvps27Δ</i> ^d	BY4742 <i>sit4::KanMX4 vps27::MXHIS3</i>	This study
BY4741 Rho0	BY4741 Rho0	[50]

Cells harboring ^a YCpHAC33-*Prom-VPS27-3xHA*, ^b pRS416-*GFP-ATG8*, ^c pYX242-*mtPho*, ^d pRS416-*MUP1-GFP*, ^e pRS426-*GFP-PHO8*, and ^f pVT100U-*preSU9-GFP* are indicated.

To assess the growth in respiratory medium, cells were grown in YPD [1% (*w/v*) yeast extract (Liofilchem, Roseto degli Abruzzi, Italy), 2% (*w/v*) peptone (Liofilchem, Roseto degli Abruzzi, Italy), and 2% (*w/v*) glucose (Thermo Fisher Scientific, Waltham, MA, USA)] or YPG [1% (*w/v*) yeast extract (Liofilchem, Roseto degli Abruzzi, Italy), 2% (*w/v*) peptone (Liofilchem, Roseto degli Abruzzi, Italy), and 3% (*v/v*) glycerol (Thermo Fisher Scientific, Waltham, MA, USA)] supplemented with 1.5% (*w/v*) agar (Liofilchem, Roseto degli Abruzzi, Italy).

The deletion of *VPS27* was carried out using a deletion fragment encompassing *KanMx4* or *MXHIS3* and *VPS27* flanking regions. Yeast cells were transformed by the lithium acetate/single-stranded carrier DNA/PEG method [51], and gene deletion was validated using standard PCR procedures.

2.2. Isolation of Vacuolar Membranes and Proteomic Analysis by HPLC-MS/MS

Cells were cultured to the late exponential (Log) phase ($OD_{600nm} \approx 2$) and vacuolar membranes were isolated as described [52,53]. Samples were processed for proteomics analysis and proteins were identified and quantified by mass spectrometry (nanoLC-MS/MS), as described [54,55]. Proteomic datasets were analyzed using Proteome Discoverer 2.5.0.400 software (Thermo Fisher Scientific, Waltham, MA, USA), the UniProt database for the *S. cerevisiae* Proteome 2020_03, and a contaminant database from MaxQuant (version 1.6.2.6, Max Planck Institute of Biochemistry, Munich, Germany). The levels of peptides were normalized based on total peptide levels of annotated vacuolar membrane proteins.

To assess group differences in protein levels, the homogeneity of variances was evaluated using the Levene test, and pairwise comparisons were conducted using Student's *t*-test. Statistical analysis was carried out using the Statistical Package for the Social Sciences (SPSS), version 26 (IBM Corp., Armonk, NY, USA), with the significance levels set at $\alpha = 0.05$. For the statistical analysis of the overrepresentation of functional groups, the Gene Ontology (GO) database (6 March 2023 and 10.5281/zenodo.7709866) was utilized.

2.3. Chronological Lifespan

CLS was evaluated as described [56]. To study the effect of iron chelation on CLS, the growth medium was supplemented with 80 μ M bathophenanthrolinedisulfonate (BPS; disodium salt hydrate; Sigma Aldrich, St. Louis, MO, USA). Cells were grown overnight in SC medium, supplemented or not with BPS, diluted to an $OD_{600nm} = 0.2$ in SC medium and further grown for 24 h (considered time zero, t_0 , in the lifespan assay). These cultures were kept at 26 °C, and cell viability was assessed over time using standard dilution plate counts on YPD medium supplemented with 1.5% (*w/v*) agar (Liofilchem, Roseto degli Abruzzi, Italy). Following incubation at 26 °C for 2–3 days, colonies were counted and the percentage of the colony-forming units (CFUs) relative to t_0 was determined.

2.4. Glucose and Ethanol Determination

Cells were grown in SC medium, and samples from the extracellular medium were taken at 12, 15, 24, and 48 h of growth after the Log phase. Glucose levels were quantified using the D-Glucose GOD-POD kit (Nzytech, Lisbon, Portugal) following the method described in the manufacturer's instructions. For ethanol determination, samples were diluted 100-fold with H_2O , and ethanol levels were quantified using the Enzytec Liquid Ethanol kit (r-biopharm, Darmstadt, Germany) following the method described in the manufacturer's instructions.

2.5. Glycogen Measurement

Cells were grown for 3 days in YPD plates and glycogen accumulation was qualitatively measured by exposing yeast colonies to iodine crystals. Yeast colonies develop a brown coloration that reflects their glycogen content [57].

2.6. Western Blotting

Cells were collected at the Log ($OD_{600nm} \approx 0.6$), late Log ($OD_{600nm} \approx 2$), and post-diauxic shift (PDS; 24 h after Log) phases, as indicated in figure legends. For the analysis of microautophagy induction, Log phase cells treated for 4 h with 200 ng mL^{-1} of rapamycin were used as positive control. Proteins were extracted using 0.1 M NaOH (Merck, Darmstadt, Germany), dissolved in Laemmli buffer, and quantified using the Pierce BCA Protein Assay Kit (Thermo Fisher Scientific, Waltham, MA, USA), as described [53]. Protein samples were prepared by adding 5% (*v/v*) 2-mercaptoethanol (Merck, Darmstadt, Germany), separated by SDS-PAGE, and transferred onto a nitrocellulose membrane (GE Healthcare, Chicago, IL, USA). For Mup1-GFP detection, cells were vortexed in Laemmli buffer in the presence of zirconium beads and then incubated at 60 °C for 10 min. To assess Mup1-GFP levels in response to methionine, proteins were extracted as previously reported [58]. Cell lysis was performed by incubating the cell pellets in 0.5 mL of 0.2 M NaOH (Merck, Darm-

stadt, Germany), 0.2% (*v/v*) 2-mercaptoethanol (Merck, Darmstadt, Germany) for 10 min on ice and adding 5% (*w/v*) trichloroacetic acid (Thermo Fisher Scientific, Waltham, MA, USA), followed by a 10 min incubation on ice. The pellet was collected by centrifugation, washed twice with acetone (Vidrolab 2, Gandra, Portugal), suspended in Laemmli buffer plus zirconium beads, vortexed, and then incubated for 10 min at 37 °C.

Immunodetection was performed using mouse anti-HA (1:1000; Santa Cruz Biotechnology, Dallas, TX, USA, sc-7392), mouse anti-GFP (1:5000; Roche, Basel, Switzerland, 11814460001), mouse anti-CPY (1:2000; Invitrogen, Waltham, MA, USA, A-6428), goat anti-ApeI (1:200; Santa Cruz Biotechnology, Dallas, TX, USA, sc-26740), mouse anti-Por1 (1:5000; Invitrogen, Waltham, MA, USA, 459500), rabbit anti-Atp2 (1:2000; Abcam, Cambridge, UK, ab128743), or mouse anti-Cox2 (1:7000; Invitrogen, Waltham, MA, USA, 4B12A5) as primary antibodies, and anti-rabbit IgG-peroxidase (1:5000; Sigma Aldrich, St. Louis, MO, USA), anti-mouse IgG-peroxidase (1:5000; Molecular Probes, Eugene, OR, USA), or anti-goat IgG-peroxidase (1:5000; Sigma Aldrich, St. Louis, MO, USA) as secondary antibodies. The primary antibodies used to probe the loading controls were mouse anti-Hxk2 (1:100,000, Rockland, Philadelphia, PA, USA, 200-4159) or mouse anti-GAPDH (1:30,000, Proteintech, Sankt Leon-Rot, Germany, 60004-1). The secondary antibody was anti-mouse IgG-peroxidase (1:5000, Molecular Probes, Eugene, OR, USA). Immunodetection was performed by chemiluminescence (ECL, Advansta, San Jose, CA, USA).

2.7. Colony Immunoblot Assay

Yeast cultures were diluted to OD_{600nm} of 0.15 using phosphate-buffered saline (PBS, 137 mM NaCl (Thermo Fisher Scientific, Waltham, MA, USA), 2.7 mM KCl (Merck, Darmstadt, Germany), 10 mM Na₂HPO₄ (Panreac, Barcelona, Spain), 1.8 mM KH₂PO₄ (Panreac, Barcelona, Spain), pH 7.4), and 13.3 µL of culture was spotted onto a SC glucose plate. Upon 72 h of incubation at 26 °C, colonies were covered with a nitrocellulose membrane (GE Healthcare, Chicago, IL, USA). After 24 h at 26 °C, membranes were removed and washed with TBS-0.05% (*v/v*) Tween (Sigma Aldrich, St. Louis, MO, USA) solution to clear away all cells that remained attached. Detection of CPY secretion was carried out by immunoblotting, with mouse anti-CPY primary antibody (1:2000, Invitrogen, Waltham, MA, USA) and anti-mouse IgG-peroxidase secondary antibody (1:5000, Molecular Probes, Eugene, OR, USA).

2.8. Iron Levels

Total iron levels were quantified in yeast cells (6×10^8 cells mL⁻¹) grown in SC glucose medium to late Log (OD_{600nm} ≈ 2) and PDS phases, using a colorimetric assay, as previously described [59].

2.9. Oxidative Stress Resistance

For the analysis of oxidative stress resistance, cells were grown to Log phase in SC medium supplemented or not with 80 µM BPS, and then treated with 1.5 mM hydrogen peroxide (H₂O₂; Merck, Darmstadt, Germany) for 1 h. Cell viability was determined as described above.

2.10. Growth Analysis

Respiratory capacity was assessed by evaluating cell growth in glycerol medium. Yeast cultures were diluted to OD_{600nm} = 0.1, and four ten-fold serial dilutions were prepared in PBS. Then cells were spotted onto YPD (glucose) or YPG (glycerol) containing 1.5% (*w/v*) agar (Liofilchem, Roseto degli Abruzzi, Italy), and the plates were incubated at 26 °C for 2–3 days. To evaluate iron sensitivity, four ten-fold serial dilutions of each culture were spotted onto SC plates supplemented or not with iron(II) sulfate heptahydrate (10 mM, 20 mM or 25 mM; Sigma Aldrich, St. Louis, MO, USA), previously dissolved in citrate buffer [81.9 mM sodium citrate (Sigma Aldrich, St. Louis, MO, USA), 18.1 mM Citric acid (Merck, Darmstadt, Germany)], and the plates were incubated for 3 days at 26 °C.

2.11. Oxygen Consumption

Oxygen consumption rate (OCR) was measured using a Clark-type oxygen electrode coupled to an Oxygraph plus system (Hansatech, Norfolk, UK), as described [53].

2.12. Alkaline Phosphatase Assay

For the analysis of alkaline phosphatase activity, protein extracts were prepared and incubated with nitrophenylphosphate (Sigma Fast, Sigma Aldrich, St. Louis, MO, USA), as described [49].

2.13. Mitochondrial Mass

The mitochondrial mass was evaluated in cells expressing GFP fused to the mitochondrial pre-sequence preSU9 (pVT100U-*preSU9-GFP*), which has low sensitivity to the mitochondrial membrane potential [60,61]. Cells were grown to Log phase, and GFP fluorescence was assessed by flow cytometry using a BD Accuri C6 (20,000 events on the FL1 channel) and the FlowJo v10.8.1 software version (BD Life Sciences, Franklin Lakes, NJ, USA).

2.14. Analysis of Mitochondrial DNA by qPCR

Cells were grown to Log phase in SC medium, and total DNA isolated using the GeneJET Genomic DNA Purification kit (Thermo Fisher Scientific, Waltham, MA, USA), following the method described in the manufacturer's instructions. The concentration and purity of all DNA stock solutions were determined with a NanoDrop ND-1000 spectrophotometer (Thermo Fisher Scientific, Waltham, MA, USA) and DNA integrity checked on agarose gels. For each sample, the total DNA concentration was normalized to 5 ng/ μ L. For qPCR amplifications, 2 μ L of template DNA (dilution 1/250) was used with the primer pairs (0.25 μ M of each primer) listed in Table 2 and 10 μ L of iTaq Universal SYBR Green supermix (Bio-Rad, Hercules, CA, USA). qPCR tests were performed using an iCycler iQ5 real-time PCR detection system (Bio-Rad, Hercules, CA, USA) with the following settings: 95 °C for 3 min; 45 cycles of 95 °C for 15 s, 55 °C for 30 s and 60 °C for 30 s. The relative efficiency and quality of each primer pair was assessed using a 5-fold serial dilution series of the DNA (1/10, 1/50, 1/250, 1/1250, and 1/6250). Negative controls (non-template controls) were included in all qPCR tests. To exclude the formation of nonspecific products, a melting curve analysis was performed at the end of each qPCR. qPCR analysis included two independent biological replicates and four technical replicates for each DNA sample. The data obtained were analyzed using the method described by Pfaffl [62] and the CFX Maestro 2.0 (v 5.0.021.0616) software (Bio-Rad, Hercules, CA, USA), to obtain the total levels of mitochondrial DNA (mtDNA) relative to nuclear DNA in the tested strains. *ACT1* was used as a reference for nuclear DNA, and *COX1* and *COX3* were used as references for mtDNA.

Table 2. Sequences of primers used in qPCR.

Primer	Sequence
COX1 fw	CTACAGATACAGCATTTC CAAGA
COX1 rv	GTGCCTGAATAGATGATAATGGT
COX3 fw	TTGAAGCTGTACAACCTACC
COX3 rv	CCTGCGATTAAGGCATGATG
ACT1 fw	GTATGTGTAAGCCGGTTTGG
ACT1 rv	CATGATACCTTGGTGTCTTGG

2.15. Statistical Analysis

Data were analyzed using GraphPad Prism Software v10.0.0 (GraphPad Software, Boston, MA, USA). Statistical comparisons were performed using one-way ANOVA, two-way ANOVA, or Student's *t*-test as appropriate. Significance levels were represented as follows: *, $p \leq 0.05$; **, $p \leq 0.01$; ***, $p \leq 0.001$; ****, $p \leq 0.0001$.

3. Results

3.1. *Vps27* Is Enriched in the Vacuolar Membranes and Mediates the Lifespan Extension of Cells Lacking the Phosphatase *Sit4*

To investigate the impact of *Sit4* deficiency on yeast lysosome-like vacuoles, we conducted a proteomic analysis of vacuolar membranes, isolated as described [52,53] from both wild-type and *sit4* Δ cells grown in SC medium to $OD_{600nm} \approx 2$. We identified a set of 230 vacuolar membrane proteins, which represent approximately 80% of the entire vacuolar membrane proteome of *S. cerevisiae*. Proteins whose levels were altered in the *sit4* Δ vacuolar membranes are presented in Table S1. A volcano plot (Figure 1A) was used to represent the differences in protein levels. The results reveal that 22 proteins exhibited reduced abundance whereas 27 proteins showed increased abundance (Figure 1B) in the vacuolar membranes of yeast lacking *Sit4*. GO analysis on biological processes revealed an enrichment in proteins related to vacuole fusion and organization, late endosome to vacuole transport, autophagy, microautophagy, polyphosphate metabolism, and metal ion homeostasis (Figure 1C and Table S2). Among the proteins that increased the most in *sit4* Δ vacuolar membranes were *Vps27* (4.1-fold) and *Hse1* (2.2-fold), which form the endosomal sorting complex required for transport-0 (ESCRT-0).

The localization and levels of *Vps27* are regulated by *Snf1*/AMPK, which promotes *Vps27* translocation from endosomes to the vacuolar membranes at the PDS phase due to glucose depletion [63,64]. Notably, *Snf1* is activated in *sit4* Δ cells and is critical for lifespan extension in this mutant strain [35]. To assess how *SIT4* deletion affects total *Vps27* levels, *vps27* Δ and *sit4* Δ *vps27* Δ cells expressing *VPS27* fused to HA, controlled by its endogenous promoter, were grown to late Log and PDS phases, and *Vps27* levels on total protein extracts were assessed by Western blotting. In agreement with the published data [63], *Vps27* levels decreased in wild-type cells during growth from the Log to the PDS phase. At the Log phase, total *Vps27* levels were lower in the *sit4* Δ mutant in comparison to wild-type cells (Figure S1A,B). Overall, our results suggest that *Vps27* is specifically enriched in the *sit4* Δ vacuolar membranes.

ESCRT-0 plays a key role in the late endosome to vacuole transport through the MVB sorting of ubiquitinated cargo [65,66]. In recent years, it was also implicated in the microautophagy of vacuolar membrane proteins [64]. Furthermore, a large-scale study suggests that *VPS27* deletion leads to a decrease in cell survival [67]. This led us to assess the impact of *VPS27* deletion on yeast CLS. Our results show that the loss of *Vps27* had a mild negative impact on lifespan, but it abolished the lifespan extension phenotype of *sit4* Δ cells (Figure 2A,B). In fact, the longevity of *sit4* Δ *vps27* Δ cells was even lower compared to that observed in *vps27* Δ cells, indicating a strong negative genetic interaction between *SIT4* and *VPS27*. Although *sit4* Δ and *sit4* Δ *vps27* Δ cells have a slow growth phenotype (Figure S2A), it is unlikely that the differences between the CLS of the different strains are related to changes in cell growth or glucose metabolism. Indeed, 24 h after Log (considered t_0 in the CLS assay due to the rapid loss of viability observed in *sit4* Δ *vps27* Δ cells), all strains clearly entered the PDS phase, as shown by the growth curve, extracellular glucose (very low or absent), and ethanol (produced at similar levels) (Figure S2A–C). Moreover, *sit4* Δ *vps27* Δ cells did not exhibit defects in the accumulation of glycogen, a storage carbohydrate that increases in *sit4* Δ cells and is critical for CLS [68].

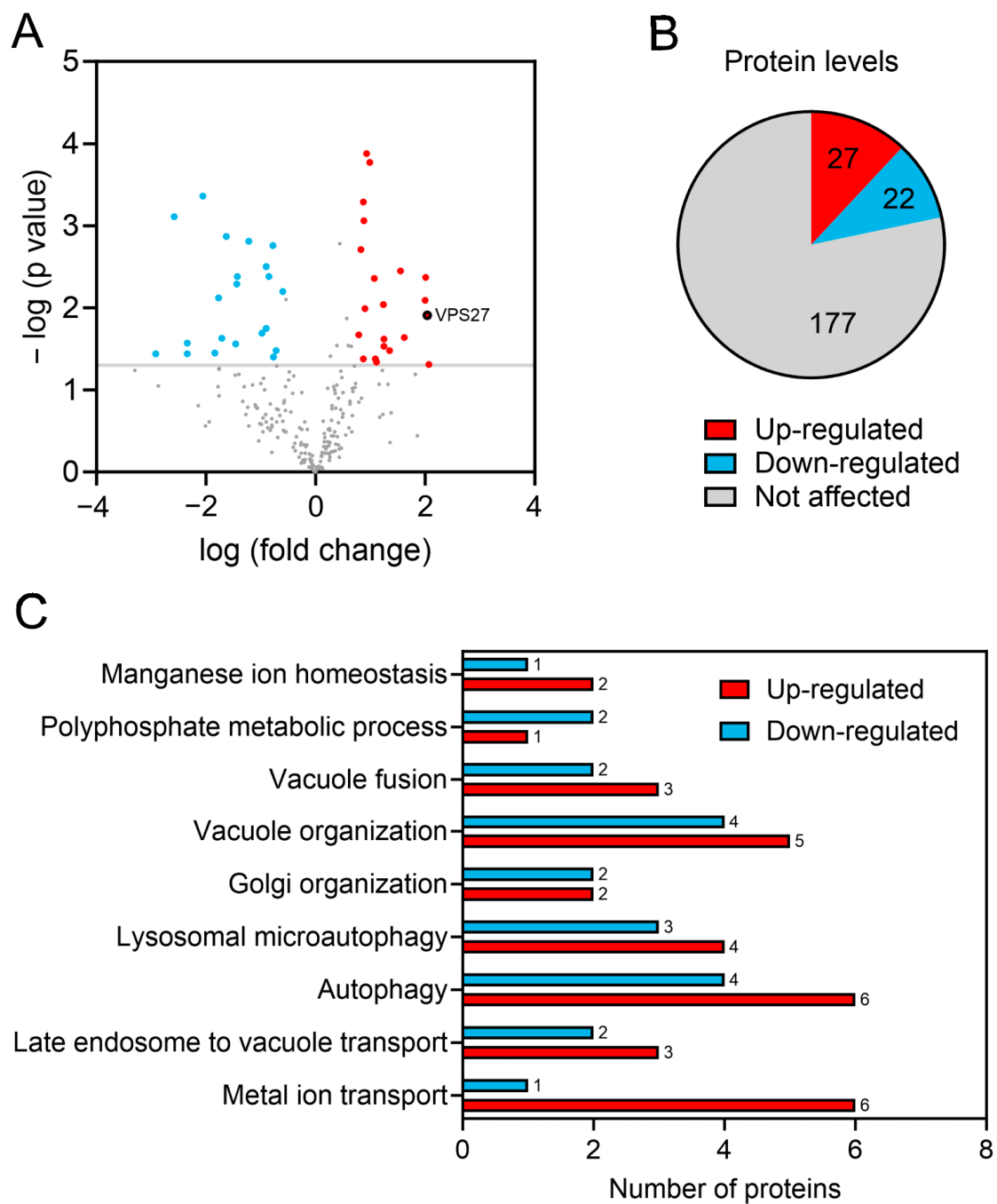


Figure 1. Proteomic analysis of *sit4Δ* vacuolar membranes. (A) Volcano plot for differentially expressed proteins in *sit4Δ* vs. wild-type samples. The log-transformed *p*-values (Student's *t*-test) are plotted in the vertical axis against the log-transformed fold change on the horizontal axis. The horizontal dashed line indicates a *p*-value of 0.05. Red dots represent proteins that are upregulated with a 1.5-fold change threshold, whereas blue dots represent proteins that are downregulated (log₂ fold change of ± 0.58). Grey dots represent the unchanged proteins. Vps27 protein is identified with a red dot with a black outline. (B) Number of proteins significantly up- or downregulated in the *sit4Δ* vacuolar membranes. (C) GO term enrichment analysis on biological processes was conducted for proteins exhibiting statistical alterations in *sit4Δ* samples.

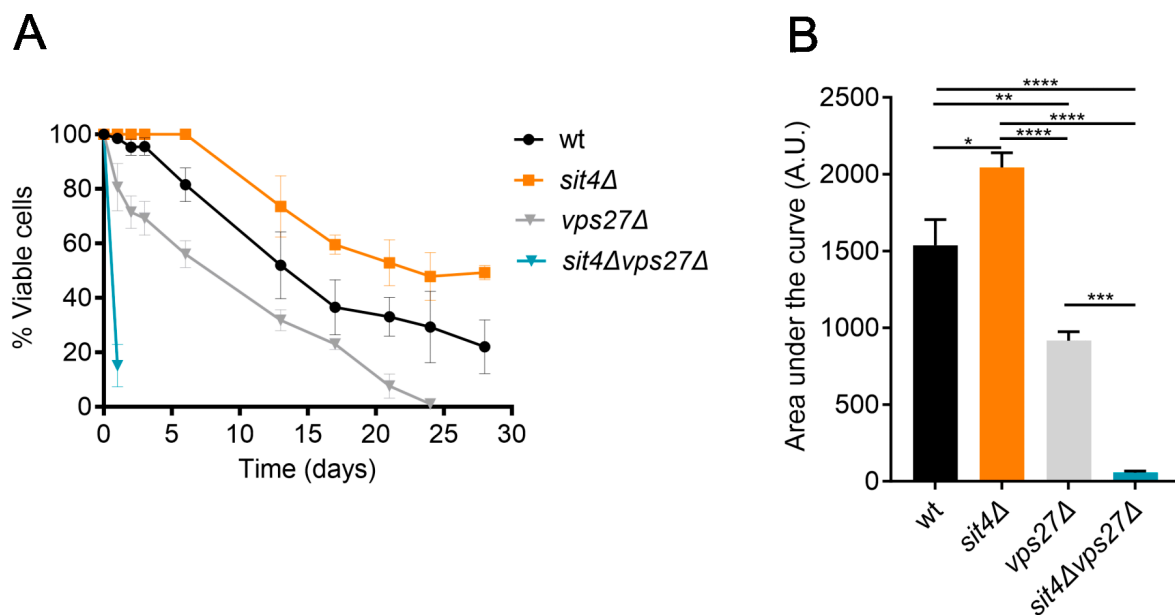


Figure 2. *SIT4* deletion extends lifespan in a *Vps27*-dependent manner. (A) Cells were grown to PDS phase (24 h after Log; t0) and maintained over time in SC medium. Cellular viability was expressed as the percentage of CFUs (aged vs. t0). Data are the mean \pm SEM ($n \geq 3$). (B) The area under each lifespan curve was calculated using GraphPad and expressed in arbitrary units (A.U.). Data are the mean \pm SEM ($n \geq 3$); * $p \leq 0.05$; ** $p \leq 0.01$; *** $p \leq 0.001$; ****, $p \leq 0.0001$; one-way ANOVA.

3.2. The Pathways for Vacuolar Degradation Are Downregulated in *sit4Δ* Cells in a *Vps27*-Independent Manner

Vps27 is involved in ubiquitinated cargo recognition and subsequently in the recruitment of ESCRT-I, facilitating the sorting of ubiquitinated MVB cargo [65,66]. During nutrient depletion, e.g., during cell growth to PDS and stationary phases, the MVB pathway promotes intracellular amino acid homeostasis and the upregulation of vacuolar hydrolases [69]. In fact, the MVB pathway synergistically cooperates with autophagy to promote cell longevity following nutrient depletion [69,70]. This led us to assess if the enrichment of *Vps27* in the *sit4Δ* vacuolar membranes results in MVB pathway induction.

To assess the MVB pathway, yeast cells were transformed with *MUP1-GFP*, to express a plasma membrane methionine permease that is transported for degradation inside vacuoles in response to starvation or to high levels of methionine [71]. When Mup1-GFP is degraded inside vacuoles, free GFP accumulates due to its resistance to the lytic environment of vacuoles. Therefore, the induction of the MVB pathway can be assessed by Western blotting, i.e., by measuring the percentage of Mup1-GFP degradation (free GFP/(Mup1-GFP + GFP) ratio). As expected, during the transition from the Log to PDS phase, the MVB pathway was induced in wild-type but not in *vps27Δ* cells (Figure 3A,B), as it is dependent on the ESCRT machinery [69,72]. In *sit4Δ* cells, Mup1-GFP degradation was significantly reduced at the PDS phase, indicating that MVB pathway induction was decreased. However, the addition of methionine increased Mup1-GFP degradation in *sit4Δ* cells to wild-type levels, in a *Vps27*-dependent manner (Figure S3), suggesting that Sit4 mediates MVB induction during cell growth but not during methionine supplementation. Overall, our data suggest that the MVB pathway does not contribute to lifespan extension in the *sit4Δ* mutant.

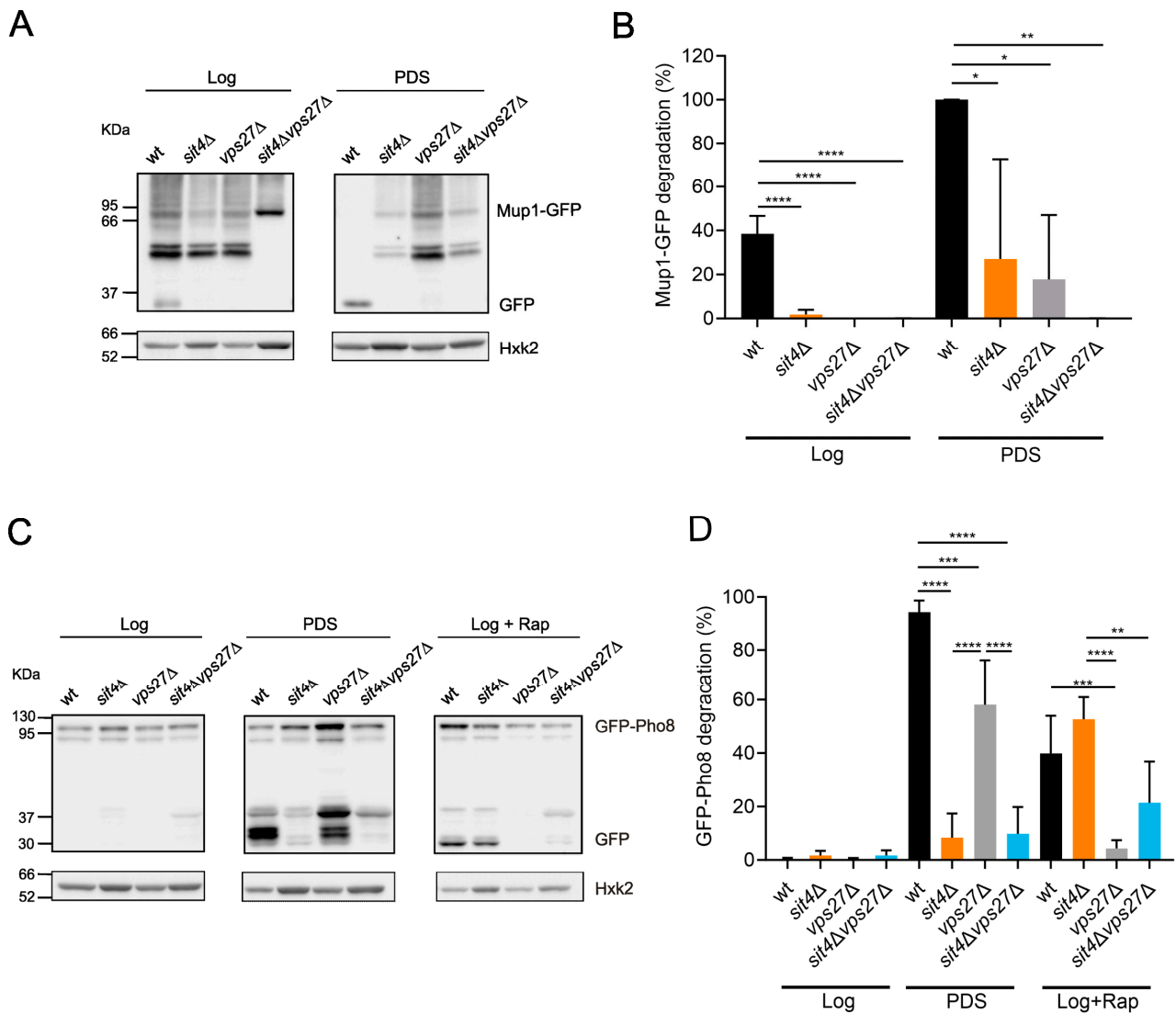


Figure 3. The induction of the MVB pathway and microautophagy at the PDS phase is Sit4-dependent. (A) Immunodetection of Mup1-GFP and GFP in protein extracts from cells expressing pRS416-*MUP1-GFP* grown in SC medium. Hxk2 was used as a loading control. A representative blot is shown. (B) The induction of the MVB pathway (free GFP/(Mup1-GFP + GFP) ratio) was evaluated at the Log and PDS (24 h after Log) phases. Values are the mean \pm SD ($n = 3$); * $p < 0.05$, ** $p < 0.01$, **** $p < 0.0001$; one-way ANOVA. (C) Immunodetection of GFP-Pho8 and GFP in protein extracts from cells expressing pRS426-*GFP-PHO8*. Hxk2 was used as a loading control. A representative blot is shown. (D) The induction of microautophagy (free GFP/(GFP + GFP-Pho8) ratio) was evaluated at the Log and PDS (24 h after Log) phases. Cells treated with rapamycin were used as a positive control. Values are the mean \pm SD ($n = 3$); ** $p < 0.01$, *** $p < 0.001$, **** $p < 0.0001$; one-way ANOVA.

Nutrient depletion also induces the sorting of vacuolar membrane proteins into the lumen followed by its degradation by microautophagy, in a Vps27-dependent manner [64,73]. This process is regulated by TORC1, as it phosphorylates Vps27 to inhibit microautophagy [74], and by Snf1, as Vps27 is incapable of reaching the vacuole in cells lacking Snf1 [63]. Microautophagy can be evaluated by following the processing of GFP-tagged Pho8 or other vacuolar membrane proteins [73,74]. To monitor microautophagy, cells were transformed with *GFP-PHO8*, and the levels of GFP-Pho8 and GFP were assessed by immunoblotting. Consistent with published findings, microautophagy was induced in wild-type cells at the PDS phase or upon TORC1 inhibition with rapamycin (Figure 3C,D) in a Vps27-dependent manner. *SIT4* deletion significantly reduced GFP-Pho8 processing at the

PDS phase, indicating that microautophagy induction was decreased in these mutant cells. However, rapamycin was capable of inducing Pho8 degradation in *sit4Δ* cells, suggesting that inhibition of microautophagy in this mutant may be caused by impaired signaling rather than defects in the machinery assisting this process. Overall, these results suggest that microautophagy does not contribute to lifespan extension in the *sit4Δ* mutant.

In the CPY pathway, the transport of proteins to vacuoles depends on multivesicular endosomes and Vps27 [75,76]. To assess if Vps27 enrichment at vacuolar membranes reflects an altered capacity of the CPY pathway in the *sit4Δ* background, CPY processing was analyzed by immunoblotting. The results showed complete processing of CPY in both growth phases in all strains (Figure 4A). However, compared with the parental strain, *vps27Δ* and *sit4Δvps27Δ* cells had a tendency to display lower levels of mature CPY (mCPY) in the Log phase (Figure 4A,B). This decrease is probably due to an aberrant secretion of the precursor form of CPY (prCPY) to the extracellular space, characteristic of class E vps mutants [77]. At the PDS phase, mCPY levels in *vps27Δ* mutants were restored to wild-type levels, suggesting that other trafficking pathways may be rescuing prCPY to be processed in the vacuole. We also assessed whether deletion of *VPS27* in *sit4Δ* cells results in a CPY secretion phenotype by performing a colony immunoblot assay. As expected, *vps27Δ* cells exhibited a strong CPY secretion phenotype (Figure 4C). Notably, CPY secretion increased in the *sit4Δvps27Δ* double mutant vs. wild-type and *sit4Δ* cells. These findings suggest that the CPY pathway is not altered in *sit4Δ* cells but that *VPS27* deletion impairs this pathway, which may underlie the premature aging of *sit4Δvps27Δ* cells.

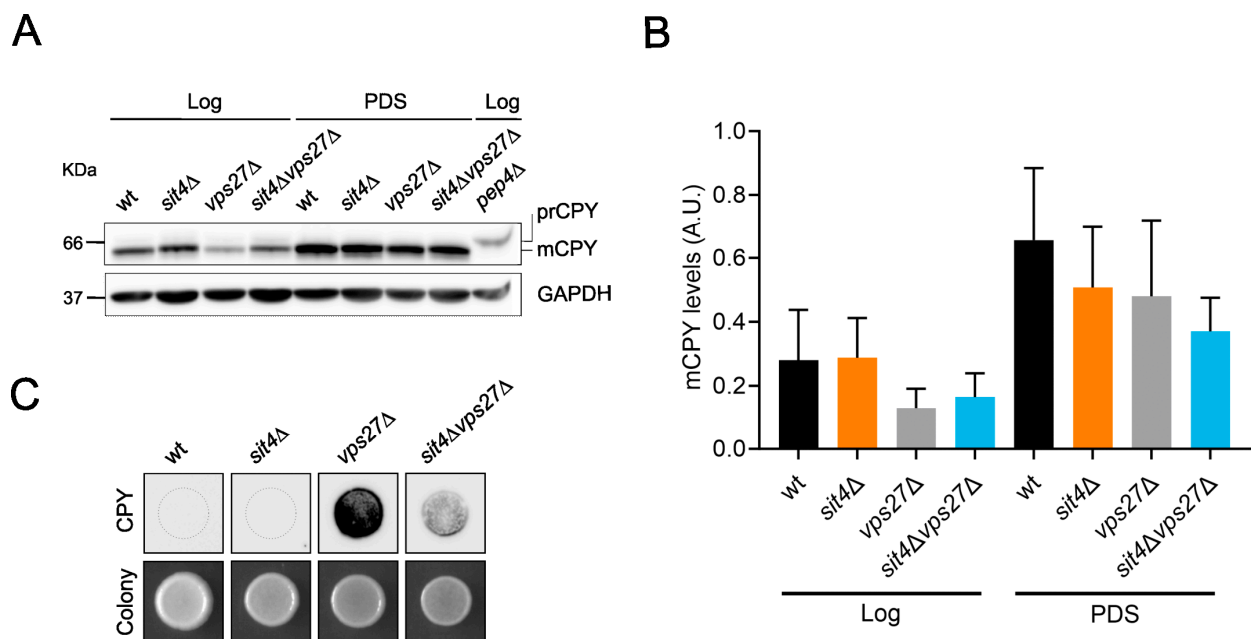


Figure 4. *VPS27* deletion impairs the CPY pathway in the *sit4Δ* mutant. (A) Immunoblotting showing complete processing of CPY in both Log and PDS (24 h after Log) phases in all strains (except in *pep4Δ* cells, used as control). (B) CPY protein levels were quantified using GAPDH as a loading control. Values are the mean \pm SD ($n = 4$). (C) CPY secretion was assessed using a colony immunoblot assay. A representative image is shown ($n = 3$).

In addition to CPY, yeast uses the Cvt pathway, another biosynthetic trafficking pathway, to transport hydrolases, such as the Ape1, into the vacuole. For this, Cvt relies on the molecular machinery involved in autophagy [30]. To determine whether Cvt is altered in *sit4Δ* cells, we monitored Ape1 processing to its mature form. In the PDS phase, all strains exhibited near complete processing of Ape1 (Figure 5A,B). However, in the Log phase, *sit4Δ* cells had a 1.7-fold increase in Ape1 maturation compared to the parental strain. Moreover,

ApeI processing increased in the *sit4Δvps27Δ* mutant vs. *vps27Δ* cells, suggesting that the deletion of *SIT4* increased the Cvt pathway in a *Vps27*-independent manner.

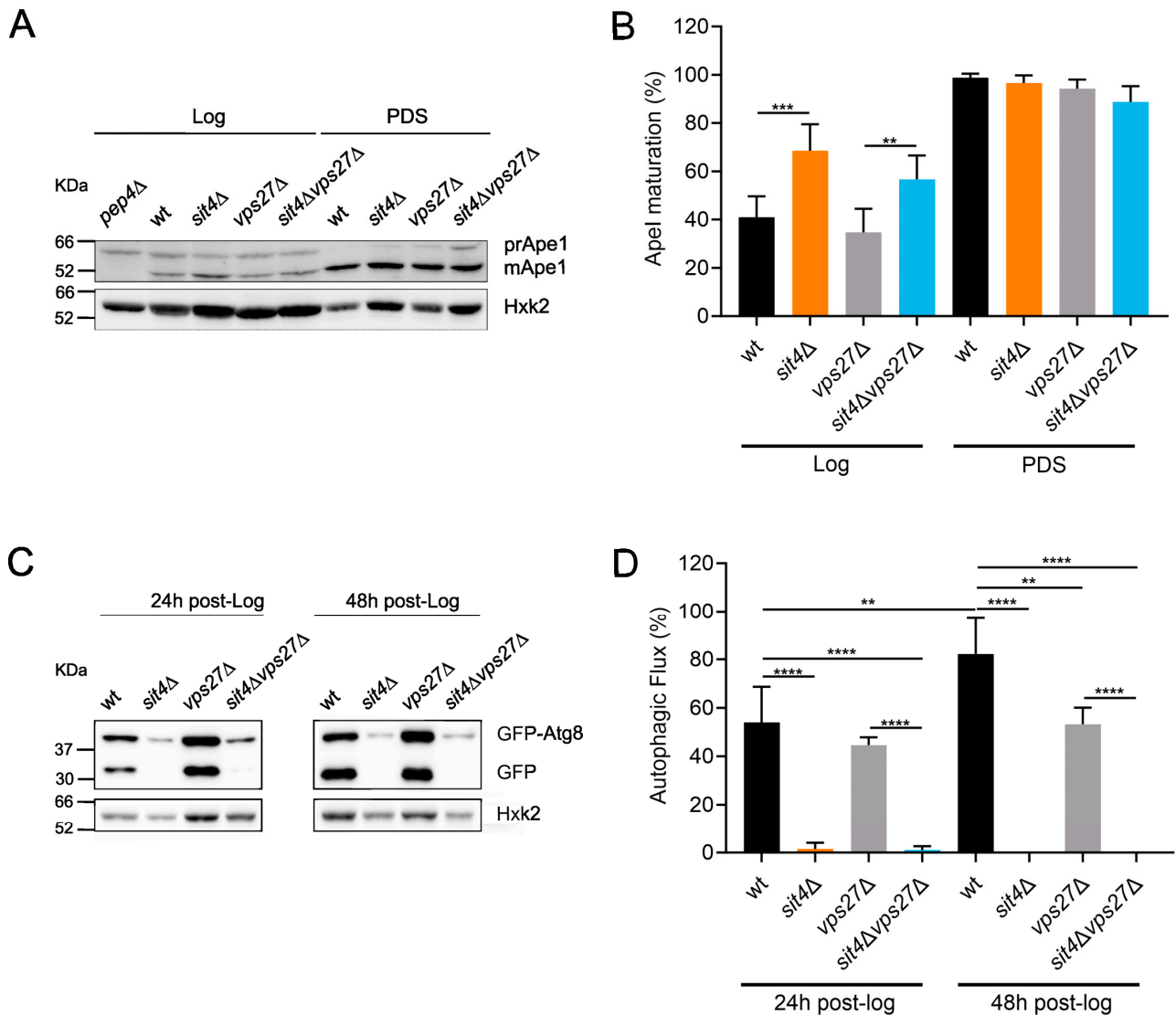


Figure 5. *SIT4* deletion compromises autophagy and induces the Cvt pathway at the Log phase in a *Vps27*-independent manner. (A) Processing of the proenzyme ApeI (prApeI) to the mature enzyme (mApeI) was analyzed at the Log and PDS (24 h after Log) phases. Hxk2 was used as a loading control. The *pep4Δ* cells (unable to process ApeI) were used as control. A representative blot is shown. (B) Quantification of ApeI maturation. Values are the mean \pm SD ($n = 4$); ** $p < 0.01$, *** $p < 0.001$; one-way ANOVA. (C) Immunodetection of GFP-Atg8 and GFP in cells expressing pRS416-GFP-ATG8. Hxk2 was used as a loading control. A representative blot is shown. (D) The autophagic flux (free GFP/(GFP + GFP-Atg8) ratio) was evaluated at 24 h and 48 h after the Log phase. Values are the mean \pm SD ($n = 3$); ** $p < 0.01$, **** $p < 0.0001$; one-way ANOVA.

Previous studies showed that yeast ESCRT mutants exhibit autophagy defects, probably associated with a decrease in ESCRT-assisted closure of the phagophore structure, leading to the formation of the autophagic body [78]. The deletion of ESCRT-0 components (*VPS27* and *HSE1*) in the fungus *Magnaporthe oryzae* also results in abnormal autophagy [79]. Since autophagy is vital for cellular homeostasis during aging [80], we also monitored the autophagic flux by employing the GFP-Atg8 cleavage assay [81]. For this, cells were transformed with *GFP-ATG8* and the levels of GFP-Atg8 and GFP were monitored during

cell growth (24 h and 48 h after the Log phase). As expected, the *vps27Δ* mutant exhibited a decreased autophagic flux. Furthermore, the autophagic flux was impaired in *sit4Δ* and *sit4Δvps27Δ* cells (Figure 5C,D) at least up to 48 h after the Log phase. The observed inhibition of autophagy in *sit4Δ* cells appears to result from changes in signaling and not from defects in the autophagic process, since previous studies demonstrated that autophagy is induced in this mutant in response to rapamycin [33,82]. These findings suggest that the increased CLS in the *sit4Δ* mutant is unrelated to autophagy.

3.3. Loss of Iron Homeostasis in *sit4Δvps27Δ* Cells Does Not Contribute to Its Shortened Lifespan

Our proteomic analysis from *sit4Δ* vacuolar membranes also identified alterations in proteins involved in iron trafficking, namely in Smf3, Ccc1, and Fth1 (Tables S1 and S2). It is known that Vps27 impacts iron homeostasis by controlling the degradation of iron transporters. Under high iron conditions, iron transporters are sorted into vesicles by ESCRT-0 and the MVB pathway, to be degraded in vacuoles [83]. This prompted us to investigate whether *VPS27* deletion affects iron homeostasis, contributing to the shortened CLS of *sit4Δvps27Δ* cells. The results showed that iron levels were similar in all strains at the Log phase (Figure 6A). However, at the PDS phase, the *sit4Δvps27Δ* mutant exhibited higher levels of iron. This result led us to evaluate the sensitivity of cells to grow in medium supplemented with iron. We found that *sit4Δ* cells exhibited a higher sensitivity to iron supplementation that was aggravated by *VPS27* deletion (Figure 6B). *VPS27* deletion in *sit4Δ* cells may decrease the degradation of iron transporters, leading to the observed high iron levels and iron sensitivity. We hypothesized that iron accumulation leads to iron toxicity, contributing to the premature aging of *sit4Δvps27Δ* cells. To examine this, we evaluated the impact of iron chelation with BPS, known to cause intracellular iron deprivation, on oxidative stress resistance and CLS. To assess oxidative stress resistance, cells grown in SC medium with or without BPS were treated with 1.5 mM H₂O₂. Our data show that *sit4Δvps27Δ* cells did not exhibit increased sensitivity to H₂O₂ (Figure 6C). Moreover, BPS decreased the H₂O₂ sensitivity in all strains, but this protective effect was lower in *sit4Δvps27Δ* mutant cells, suggesting that iron accumulation does not aggravate H₂O₂ sensitivity. Moreover, BPS had a minor effect on the CLS of *sit4Δvps27Δ* cells as it only increased cell survival from 1 to 2 days (Figure 6D). Overall, these findings suggest that iron accumulation does not seem to be a primary contributing factor to the drastic viability loss of *sit4Δvps27Δ* cells.

3.4. Vps27 Is Crucial for Mitochondrial Function in *sit4Δ* Cells

Sit4 regulates mitochondrial metabolism by repressing respiratory genes in high glucose conditions [42], and mitochondrial derepression is crucial for the increased CLS of *sit4Δ* cells [32,34,35]. Sit4 modulates the catabolite repression through regulation of Mig1 and Hxk2. During cellular growth in a glucose medium, the unphosphorylated Mig1-Hxk2 complex accumulates in the nucleus, where it represses the expression of genes required for cellular growth on non-fermentable carbon sources [84,85]. In the absence of Sit4, Hxk2 is hyperphosphorylated [86] and Mig1 levels decrease [87]. Moreover, Snf1 is activated [88,89], leading to Mig1 phosphorylation and inhibition [90]. Thus, cells lacking Sit4 exhibit a high oxygen consumption rate (OCR) already at the Log phase even when grown in fermentable media [32]. A higher respiratory capacity early in growth has been related to an improved tolerance to reactive oxygen species during the stationary phase and also to an increase in lifespan [91,92]. Moreover, *sit4Δ* cells exhibit a higher dependency on the respiratory metabolism than wild-type cells [42]. These data and the lack of alterations in vacuolar trafficking pathways regulated by Vps27 that may explain its role in *sit4Δ* lifespan led us to analyze the function of Vps27 in the modulation of *sit4Δ* mitochondrial function.

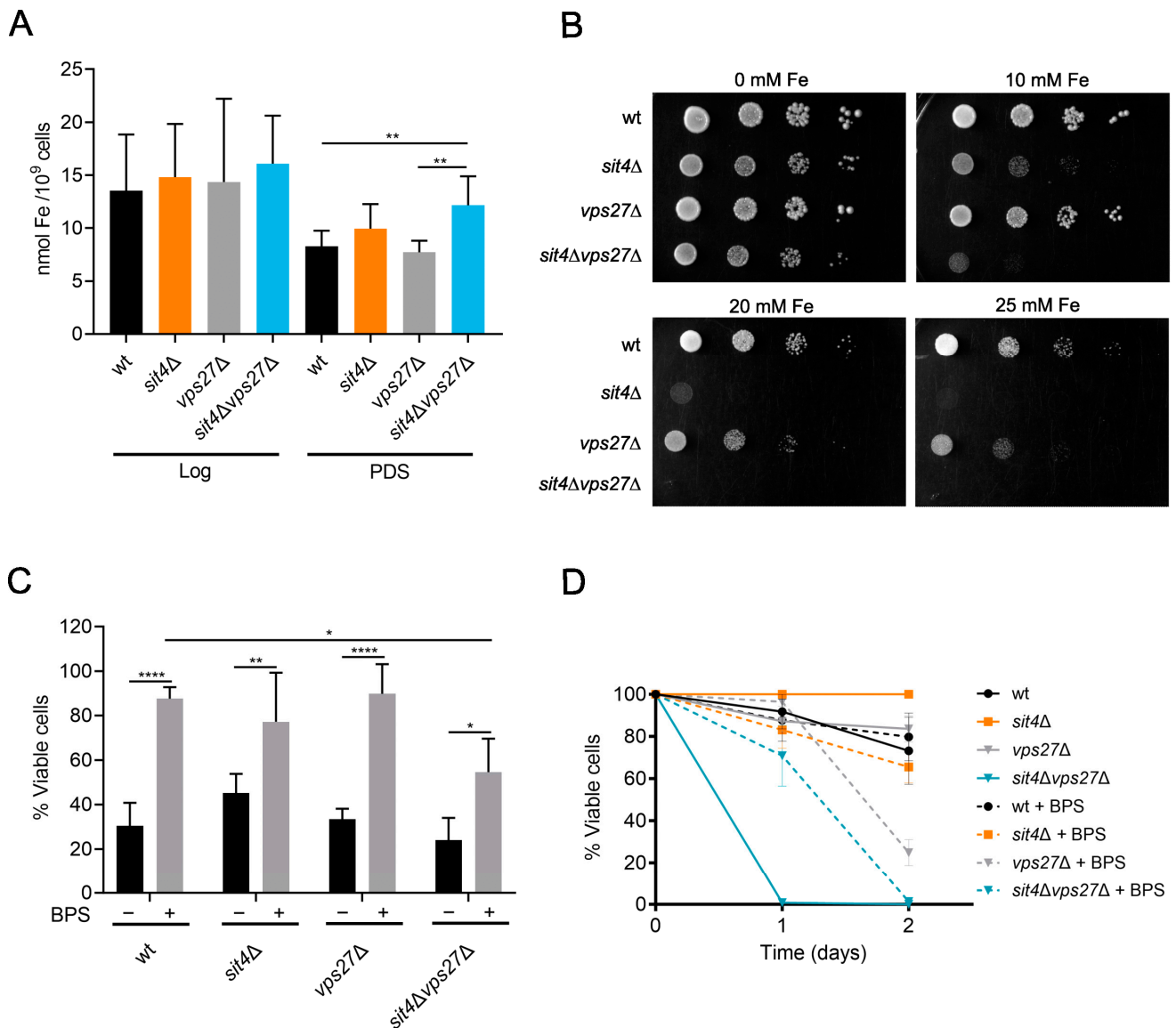


Figure 6. Iron levels and the effect of iron chelation on H₂O₂ resistance and CLS in *sit4Δvps27Δ* cells. (A) Total iron levels were quantified in cells grown to late Log and PDS (24 h after Log) phases. Values are the mean ± SD ($n \geq 6$); ** $p \leq 0.01$; one-way ANOVA. (B) Cells were grown to the Log phase and four ten-fold serial dilutions were spotted onto SC plates with or without supplementation of iron (II) sulphate heptahydrate. A representative image is shown ($n = 3$). (C) Cells were grown to Log phase in medium with or without supplementation of 80 μM of BPS and treated with 1.5 mM H₂O₂ for 1 h. Cell viability was expressed as the percentage of the CFUs (treated cells vs. non-stressed cells). Values are the mean ± SD ($n \geq 3$); * $p \leq 0.05$, ** $p \leq 0.01$, **** $p \leq 0.0001$; one-way ANOVA. (D) Cells were grown to the PDS phase (t₀) in SC medium with or without supplementation of 80 μM BPS and maintained over time in the same medium. Cellular viability was quantified as the percentage of the CFUs (aged vs. t₀). Data are the mean ± SEM ($n \geq 3$).

To assess if Vps27 is required for the increased mitochondrial respiration displayed by *sit4Δ* cells, the OCR was measured in cells at both Log and PDS phases. Notably, VPS27 deletion abolished mitochondrial derepression at the Log phase in cells lacking Sit4 (Figure 7A). In fact, *sit4Δvps27Δ* cells had lower OCR in both growth phases, compared to wild-type and *sit4Δ* cells, indicating that the double mutant has severe deficiencies in mitochondrial respiration. Furthermore, the *vps27Δ* mutant failed to fully induce mitochondrial respiration during growth from the Log to the PDS phase and exhibited a

lower OCR, compared to the parental strain. Thus, Vps27 seems to potentiate optimal mitochondrial activity, and its decrease may contribute to the shortened CLS exhibited by *vps27*Δ mutants (Figure 2). We also evaluated the ability of *sit4*Δ*vps27*Δ cells to grow in a medium containing glycerol (YPG), a respiratory carbon source, instead of glucose (YPD). The results demonstrated that *sit4*Δ*vps27*Δ cells were incapable of growing in YPG (Figure 7B), further suggesting that mitochondrial function is impaired. Overall, these results suggest that Vps27 is essential to ensure respiratory fitness and extended longevity in *sit4*Δ cells.

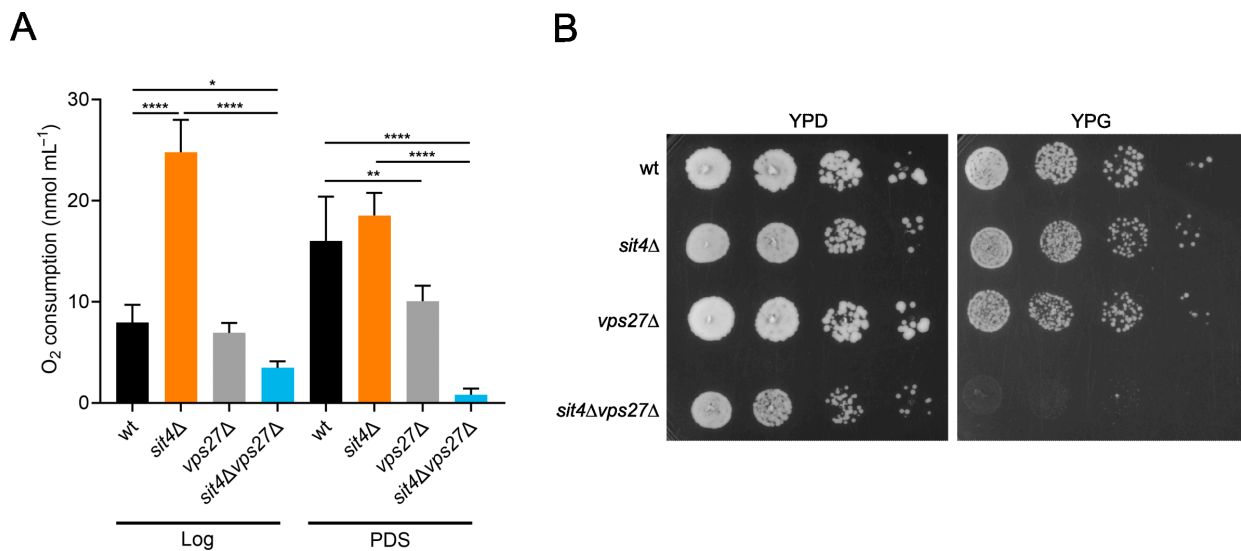


Figure 7. The *sit4*Δ*vps27*Δ mutant has impaired mitochondrial respiration. (A) Cells were grown to Log and PDS phases and mitochondrial respiration was determined by measuring oxygen consumption rate. Values are the mean \pm SD ($n \geq 4$); * $p < 0.05$, ** $p < 0.01$, **** $p < 0.0001$; one-way ANOVA. (B) Cells were grown to Log phase and four ten-fold serial dilutions were spotted onto YPD or YPG plates. A representative image is shown ($n = 4$).

Numerous studies support a key role of vacuolar trafficking pathways, such as autophagy and mitophagy, in mitochondrial fitness. Mitophagy is a selective type of autophagy that targets damaged mitochondria for degradation in vacuoles. Along with mitochondrial dynamics, mitophagy is of central importance to the sustainment of mitochondrial integrity and activity [93–96]. This led us to investigate whether Vps27 is involved in the modulation of mitophagy and mitochondrial biogenesis in cells lacking Sit4. Mitophagy was assessed in cells expressing the vacuolar alkaline phosphatase Pho8 targeted to mitochondria (mtPho8) [97]. Since maturation of the Pho8 pro-enzyme requires vacuolar Pep4, the alkaline phosphatase activity is an indicator of mitochondrial degradation in vacuoles. Our results show that the alkaline phosphatase activity was higher in cells lacking Sit4 at the Log and PDS phases, although in a Vps27-independent manner (Figure 8A). In fact, we even observed higher activity in *sit4*Δ*vps27*Δ cells at the Log phase compared to *sit4*Δ cells. This indicates that the mitochondrial respiration defects in the double mutant *sit4*Δ*vps27*Δ are not associated with impaired mitophagy. Moreover, these findings suggest that enhanced mitophagy activity in *sit4*Δ cells is not associated with Vps27-dependent CLS extension.

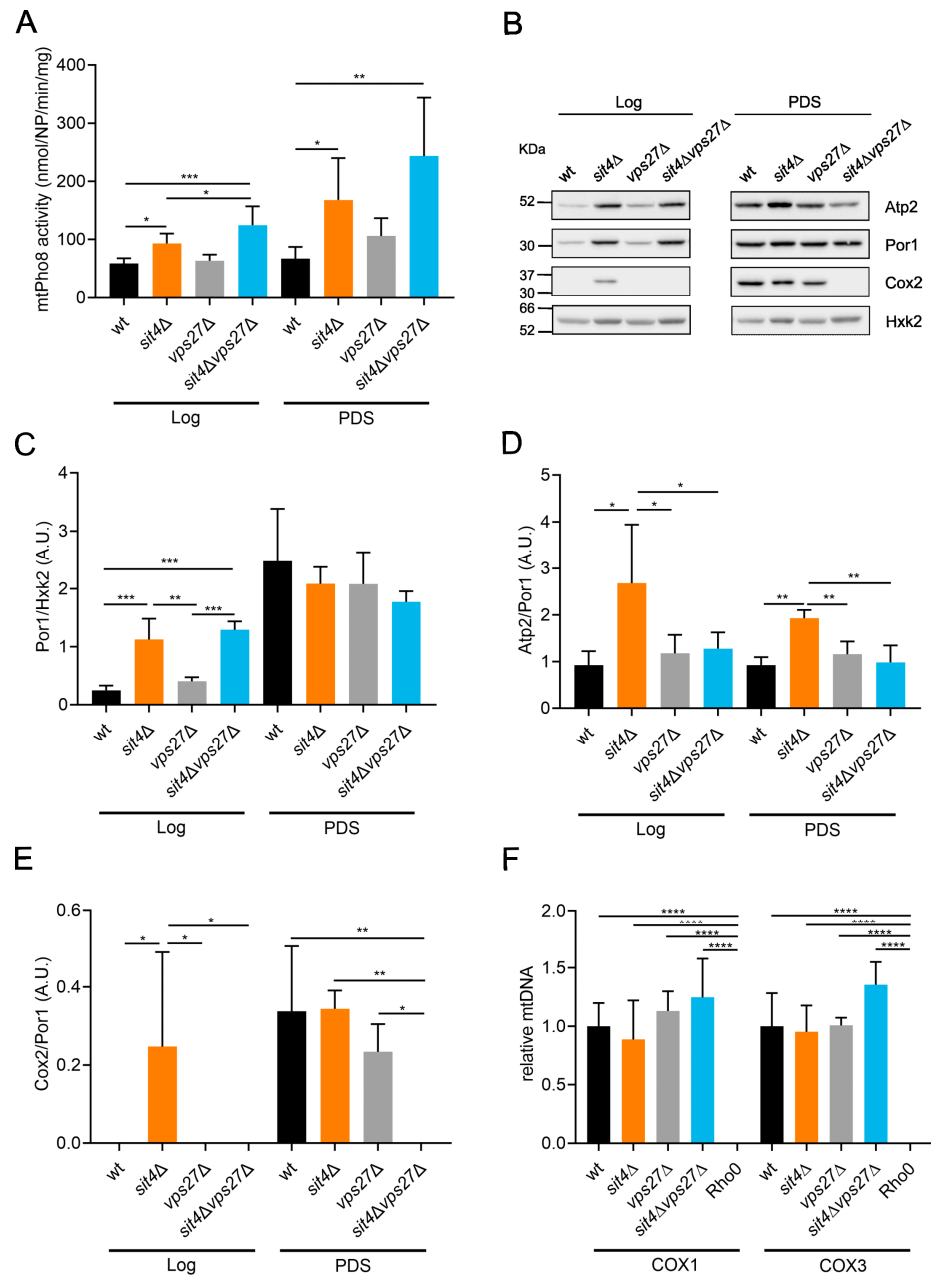


Figure 8. *VPS27* deletion in *sit4Δ* cells leads to a decrease in *Atp2* and *Cox2* levels, but it does not affect mitophagy or mitochondrial biogenesis. (A) Mitophagy is induced in *sit4Δ* cells in a *Vps27*-independent manner. Cells expressing pYX242-*mtPHO8* were grown to Log and PDS (24 h after Log) phases and mitophagy was determined by measuring the alkaline phosphatase activity. Values are the mean \pm SD ($n = 4$); * $p \leq 0.05$, ** $p \leq 0.01$, *** $p < 0.001$; one-way ANOVA. (B) Cells were grown to Log and PDS phases and the levels of mitochondrial proteins (*Por1*, *Atp2*, and *Cox2*) were assessed by immunoblotting. *Hxk2* was used as a loading control. A representative blot is shown ($n = 3$). (C) Relative amount of *Por1* (a mitochondrial outer membrane protein) to *Hxk2* is shown as an indicator of mitochondrial mass. Values are the mean \pm SD; ** $p \leq 0.01$, *** $p < 0.001$; one-way ANOVA. (D,E) Quantification of the ratio *Atp2*/*Por1* (D) and *Cox2*/*Por1* (E). Values are the mean \pm SD; * $p \leq 0.05$, ** $p \leq 0.01$; one-way ANOVA. (F) Analysis of mtDNA/nuclear DNA by qPCR. *COX1* and *COX3* were used as reference for mtDNA and *ACT1* for nuclear DNA. *Rho0* cells were used as control. Values are the mean \pm SD ($n = 4$); **** $p < 0.0001$; one-way ANOVA.

Mitochondrial integrity depends on the coordination of both mitochondrial degradation and mitochondrial biogenesis [93,94,98]. To evaluate if *VPS27* deletion affects mitochondrial biogenesis, the levels of mitochondrial proteins (Por1, Atp2, and Cox2) were assessed in cells at the Log and PDS phases. As expected, the levels of the porin Por1 increased in wild-type cells from the Log to the PDS phase (Figure 8B,C), reflecting the higher mitochondrial mass characteristic of the respiratory phase. Accordingly with the early catabolite derepression in cells lacking Sit4, the levels of Por1 increased at the Log phase. The increase in mitochondrial biogenesis in the *sit4Δ* mutant was Vps27 independent, as *sit4Δvps27Δ* also exhibited higher levels of Por1 at the Log phase. Similar changes were observed when mitochondrial mass was assessed by flow cytometry, using cells expressing preSU9-GFP (Figure S2). Notably, deletion of *VPS27* in *sit4Δ* cells abolished the higher levels of the oxidative phosphorylation proteins Atp2 and Cox2 (Figure 8B,D,E). In fact, Cox2 was not detected in *sit4Δvps27Δ* cells, even at the PDS phase. As Cox2 is encoded by the mitochondrial genome, we speculated that *sit4Δvps27Δ* exhibits defects in the maintenance of mtDNA. However, analysis by qPCR revealed that mtDNA levels were not affected in *sit4Δvps27Δ* compared to wild-type cells (Figure 8F). These observations suggest that the defects in *sit4Δvps27Δ* mitochondrial function did not result from defects in mitochondrial biogenesis or the loss of mtDNA.

4. Discussion

The decline in the function of lysosomes (vacuoles in yeast) and mitochondria has been linked to the aging process and the development of age-related diseases [1,6]. Furthermore, numerous interventions that improve the function of these organelles also increase lifespan [7,12–18]. Our previous studies showed that *SIT4* deletion increases mitochondrial respiration and yeast CLS, in part mediated by increased phosphorylation levels of hexokinase 2 [86] and ATP synthase catalytic beta subunit Atp2 [34], as well as Snf1/AMPK activation [35]. The deletion of *SIT4* also suppresses the mitochondrial dysfunction exhibited by Isc1-deficient cells that accumulate ceramide during aging [32], as well as the vacuolar fragmentation and dysfunctions exhibited by this mutant [33]. However, the mechanism by which Sit4 regulates the vacuolar–mitochondrial axis is not fully understood, and its characterization may help to define new strategies to improve lifespan.

In this study, we identified 49 vacuolar membrane proteins whose levels change in cells lacking Sit4. These proteins were mainly associated with cellular processes, such as vacuole fusion and organization, late endosome to vacuole transport, autophagy, microautophagy, polyphosphate metabolism, and metal ion homeostasis. Proteins that increased significantly in *sit4Δ* vacuolar membranes include Vps27 (4.1-fold) and Hse1 (2.2-fold), components of the ESCRT-0 [65]. The enrichment of Vps27 at *sit4Δ* vacuolar membranes was not due to upregulation of Vps27 since its total protein levels were not increased. The translocation of Vps27 from endosomes to vacuolar membranes depends on Snf1 activity at the PDS phase [63] and Sit4 deficiency results in Snf1 activation early during growth in glucose medium [88,89]. Whether Snf1 activation promotes Vps27 vacuolar localization in *sit4Δ* cells remains to be clarified.

Our results suggest that Vps27 is crucial for lifespan extension in *sit4Δ* cells. Indeed, the CLS of *sit4Δvps27Δ* cells was much shorter than that of each single mutants, indicating a negative genetic interaction between *SIT4* and *VPS27*. The analysis of vacuolar trafficking pathways that are known to be dependent on Vps27 showed that the MVB pathway and microautophagy were impaired in both *sit4Δ* and *sit4Δvps27Δ* cells. However, *VPS27* deletion in *sit4Δ* cells resulted in aberrant CPY secretion. Thus, defects in the transport of cargo proteins through the CPY pathway may contribute to vacuolar dysfunction and a short lifespan in *sit4Δvps27Δ* cells. We also showed that the Cvt pathway was induced in both *sit4Δ* and *sit4Δvps27Δ* cells at the Log phase, suggesting that Vps27 does not promote *sit4Δ* CLS through regulation of Cvt. Intriguingly, the induction of autophagy at the PDS phase was impaired in *sit4Δ* and *sit4Δvps27Δ* cells. Autophagy induction has been largely associated with increased longevity and described as a requirement for lifespan

extension by pharmacological and nutritional interventions [24,99]. However, several *atg* mutants with defective autophagy still exhibit lifespan extension under caloric restriction conditions [100]. Furthermore, several pieces of evidence suggest that autophagy and the ubiquitin proteasome system are coordinated for proper control of protein homeostasis and housekeeping functions, and that the inhibition of autophagy can be compensated by the induction of the proteasome, and vice versa [101–104]. Although Sit4 does not regulate proteasome activity, Sit4 and proteasome are functionally linked as they act in concert in osmoregulation and nutrient sensing [105]. More studies are required to assess if the ubiquitin proteasome system contributes to *sit4Δ* lifespan extension.

Our studies also suggest that Vps27 contributes to iron homeostasis, with *sit4Δvps27Δ* cells accumulating high iron levels and exhibiting increased sensitivity to iron supplementation. However, iron accumulation does not seem to be involved in the *sit4Δvps27Δ* premature aging, as BPS treatment only promoted a minor increase in the mutant CLS. In addition, we found that Vps27 affects the levels of proteins critical for oxidative phosphorylation in *sit4Δ* cells, namely of Atp2 and Cox2. How Vps27 regulates these proteins in cells lacking Sit4 to increase mitochondrial fitness, which is critical for the *sit4Δ* mutant extended longevity, requires further investigation.

5. Conclusions

In summary, this study suggests that Vps27, a component of the ESCRT-0 complex, is enriched at the vacuolar membrane of *sit4Δ* cells, playing a crucial role in the CLS extension observed in this mutant strain. Interestingly, the deletion of *VPS27* in *sit4Δ* cells did not affect protein trafficking or vacuolar sorting pathways. However, it impaired mitochondrial respiration, associated with reduced levels of Atp2 and Cox2. Together, these findings unveil a novel link between Sit4, Vps27, and mitochondrial respiration, providing valuable insights into the intricate mechanisms governing cellular longevity.

Supplementary Materials: The following supporting information can be downloaded at: <https://www.mdpi.com/article/10.3390/cells13080655/s1>, Figure S1: *SIT4* deletion decreases Vps27 levels at the Log phase; Figure S2: Growth and metabolic profile of indicated strains; Figure S3: Methionine increases Mup1-GFP degradation in *sit4Δ* cells; Figure S4: Mitochondrial mass increases in *sit4Δ* and *sit4Δvps27Δ* cells; Figure S5: Original images of Western blots used for data quantification displayed in Figure 3A,B; Figure S6: Original images of Western blots used for data quantification displayed in Figure 3C,D; Figure S7: Original images of Western blots used for data quantification displayed in Figure 4A,B; Figure S8: Uncropped and unadjusted original image of the colony immunoblot displayed in Figure 4C; Figure S9: Original images of the Western blots used for the data quantification displayed in Figure 5A,B; Figure S10: Original images of Western blots used for the data quantification displayed in Figure 5C,D; Figure S11: Original images of Western blots used for the data quantification displayed in Figure 8B–E; Figure S12: Original images of Western blots used for the data quantification displayed in Figure S1A,B; Figure S13: Uncropped and unadjusted original image of the yeast colonies exposed to iodine vapor to qualitatively evaluate the glycogen content displayed in Figure S2D; Table S1: Levels of vacuolar membrane proteins in wild-type and *sit4Δ* samples; Table S2: Gene Ontology (GO) enrichment analysis on biological processes.

Author Contributions: Conceptualization, T.S.M., C.P. and V.C.; methodology, T.S.M., M.C., D.P. and M.V.M.; formal analysis, T.S.M., M.C., D.P., C.L., M.V.M., C.P. and V.C.; investigation, T.S.M., M.C. and D.P.; resources, T.S.M., M.V.M., C.P. and V.C.; data curation, T.S.M., M.C., D.P., C.L., M.V.M., C.P. and V.C.; writing—original draft preparation, T.S.M.; writing—review and editing, T.S.M., M.C., D.P., C.L., M.V.M., C.P. and V.C.; visualization, T.S.M., M.C. and D.P.; supervision, C.P. and V.C.; project administration, V.C.; funding acquisition, V.C. All authors have read and agreed to the published version of the manuscript.

Funding: This work was funded by national funds through FCT—Fundação para a Ciência e a Tecnologia, I.P., under the project UIDB/04293/2020. T.S.M. (SFRH/BD/136996/2018 and COVID/BD/153217/2023), M.V.M. (DL57/2016/CP1355/CT0023) and C.P. (IF/00889/2015) are supported by FCT. Work at the i3S Proteomics Scientific Platform is supported by the Portuguese Mass Spectrometry Network, integrated in the National Roadmap of Research Infrastructures of Strategic Relevance

(ROTEIRO/0028/2013; LISBOA-01-0145-FEDER-022125). The i3S Advanced Light Microscopy Platform is a member of the national infrastructure PPBI—Portuguese Platform of Bioimaging (PPBI-POCI-01-0145-FEDER-022122).

Institutional Review Board Statement: Not applicable.

Data Availability Statement: The mass spectrometry proteomics data have been deposited to the ProteomeXchange Consortium via the PRIDE [106] partner repository with the dataset identifier PXD048450.

Acknowledgments: We are grateful to Paula Ludovico (ICVS, Universidade do Minho, Portugal), Helder Maiato (i3S, Universidade do Porto, Portugal), Sylvie Friant (Université de Strasbourg and Centre National de la Recherche Scientifique, Strasbourg, France), David Teis (Division of Cell Biology, Biocenter, Medical University of Innsbruck, and Austrian Drug Screening Institute, Innsbruck, Austria), Claudio de Virgilio (Department of Biology, University of Fribourg, Fribourg, Switzerland), and Benedikt Westermann (Institute for Physiological Chemistry, Ludwig Maximilian University of Munich, Munich, Germany) for providing, respectively, the pRS416-GFP-ATG8 plasmid and mouse anti-CPY antibody, the mouse anti-GAPDH antibody, the YCpHAC33-Prom-Vps27-3xHA plasmid, the pRS416-MUP1-GFP plasmid, the pRS426-GFP-PHO8 plasmid, and the plasmid pVT100U-preSU9-GFP. We also thank Hugo Osório (i3S Proteomics Scientific Platform) for his support in the proteomic analysis.

Conflicts of Interest: The authors declare no conflicts of interest. The funders had no role in the design of the study; in the collection, analyses, or interpretation of data; in the writing of the manuscript; or in the decision to publish the results.

References

- Carmona-Gutierrez, D.; Hughes, A.L.; Madeo, F.; Ruckenstein, C. The Crucial Impact of Lysosomes in Aging and Longevity. *Ageing Res. Rev.* **2016**, *32*, 2–12. [[CrossRef](#)] [[PubMed](#)]
- Lim, C.-Y.; Zoncu, R. The Lysosome as a Command-and-Control Center for Cellular Metabolism. *J. Cell Biol.* **2016**, *214*, 653–664. [[CrossRef](#)] [[PubMed](#)]
- Lamming, D.W.; Bar-Peled, L. Lysosome: The Metabolic Signaling Hub. *Traffic* **2019**, *20*, 27–38. [[CrossRef](#)] [[PubMed](#)]
- Lawrence, R.E.; Zoncu, R. The Lysosome as a Cellular Centre for Signalling, Metabolism and Quality Control. *Nat. Cell Biol.* **2019**, *21*, 133–142. [[CrossRef](#)] [[PubMed](#)]
- Li, S.C.; Kane, P.M. The Yeast Lysosome-like Vacuole: Endpoint and Crossroads. *Biochim. Biophys. Acta* **2009**, *1793*, 650–663. [[CrossRef](#)] [[PubMed](#)]
- Lloyd-Evans, E.; Haslett, L.J. The Lysosomal Storage Disease Continuum with Ageing-Related Neurodegenerative Disease. *Ageing Res. Rev.* **2016**, *32*, 104–121. [[CrossRef](#)] [[PubMed](#)]
- Martinez-Lopez, N.; Athonvarangkul, D.; Singh, R. Autophagy and Aging. *Adv. Exp. Med. Biol.* **2015**, *847*, 73–87. [[CrossRef](#)] [[PubMed](#)]
- Hughes, A.L.; Gottschling, D.E. An Early Age Increase in Vacuolar pH Limits Mitochondrial Function and Lifespan in Yeast. *Nature* **2012**, *492*, 261–265. [[CrossRef](#)] [[PubMed](#)]
- López-Otín, C.; Blasco, M.A.; Partridge, L.; Serrano, M.; Kroemer, G. The Hallmarks of Aging. *Cell* **2013**, *153*, 1194–1217. [[CrossRef](#)]
- Cuervo, A.M.; Dice, J.F. When Lysosomes Get Old. *Exp. Gerontol.* **2000**, *35*, 119–131. [[CrossRef](#)]
- Barbosa, M.C.; Grosso, R.A.; Fader, C.M. Hallmarks of Aging: An Autophagic Perspective. *Front. Endocrinol.* **2019**, *9*, 790. [[CrossRef](#)] [[PubMed](#)]
- Madeo, F.; Eisenberg, T.; Büttner, S.; Ruckenstein, C.; Kroemer, G. Spermidine: A Novel Autophagy Inducer and Longevity Elixir. *Autophagy* **2010**, *6*, 160–162. [[CrossRef](#)] [[PubMed](#)]
- Pyo, J.-O.; Yoo, S.-M.; Ahn, H.-H.; Nah, J.; Hong, S.-H.; Kam, T.-I.; Jung, S.; Jung, Y.-K. Overexpression of Atg5 in Mice Activates Autophagy and Extends Lifespan. *Nat. Commun.* **2013**, *4*, 2300. [[CrossRef](#)]
- Simonsen, A.; Cumming, R.C.; Brech, A.; Isakson, P.; Schubert, D.R.; Finley, K.D. Promoting Basal Levels of Autophagy in the Nervous System Enhances Longevity and Oxidant Resistance in Adult *Drosophila*. *Autophagy* **2008**, *4*, 176. [[CrossRef](#)] [[PubMed](#)]
- Tóth, M.L.; Sigmond, T.; Borsos, É.; Barna, J.; Erdélyi, P.; Takács-Vellai, K.; Orosz, L.; Kovács, A.L.; Csikós, G.; Sass, M.; et al. Longevity Pathways Converge on Autophagy Genes to Regulate Life Span in *Caenorhabditis elegans*. *Autophagy* **2008**, *4*, 330–338. [[CrossRef](#)] [[PubMed](#)]
- Wei, M.; Fabrizio, P.; Hu, J.; Ge, H.; Cheng, C.; Li, L.; Longo, V.D. Life Span Extension by Calorie Restriction Depends on Rim15 and Transcription Factors Downstream of Ras/PKA, Tor, and Sch9. *PLoS Genet.* **2008**, *4*, e13. [[CrossRef](#)] [[PubMed](#)]
- Mirzaei, H.; Suarez, J.A.; Longo, V.D. Protein and Amino Acid Restriction, Aging and Disease: From Yeast to Humans. *Trends Endocrinol. Metab.* **2014**, *25*, 558–566. [[CrossRef](#)] [[PubMed](#)]
- Ruetenik, A.; Barrientos, A. Dietary Restriction, Mitochondrial Function and Aging: From Yeast to Humans. *Biochim. Biophys. Acta—Bioenergy* **2015**, *1847*, 1434–1447. [[CrossRef](#)]

19. Hecht, K.A.; O'Donnell, A.F.; Brodsky, J.L. The Proteolytic Landscape of the Yeast Vacuole. *Cell. Logist.* **2014**, *4*, e28023. [[CrossRef](#)]
20. Mehrpour, M.; Esclatine, A.; Beau, I.; Codogno, P. Overview of Macroautophagy Regulation in Mammalian Cells. *Cell Res.* **2010**, *20*, 748–762. [[CrossRef](#)]
21. Wen, X.; Klionsky, D.J. An Overview of Macroautophagy in Yeast. *J. Mol. Biol.* **2016**, *428*, 1681–1699. [[CrossRef](#)] [[PubMed](#)]
22. Youle, R.J.; Narendra, D.P. Mechanisms of Mitophagy. *Nat. Rev. Mol. Cell Biol.* **2011**, *12*, 9–14. [[CrossRef](#)] [[PubMed](#)]
23. Alao, J.P.; Legon, L.; Dabrowska, A.; Tricolici, A.M.; Kumar, J.; Rallis, C. Interplays of AMPK and TOR in Autophagy Regulation in Yeast. *Cells* **2023**, *12*, 519. [[CrossRef](#)] [[PubMed](#)]
24. Aman, Y.; Schmauck-Medina, T.; Hansen, M.; Morimoto, R.I.; Simon, A.K.; Bjedov, I.; Palikaras, K.; Simonsen, A.; Johansen, T.; Tavernarakis, N.; et al. Autophagy in Healthy Aging and Disease. *Nat. Aging* **2021**, *1*, 634–650. [[CrossRef](#)] [[PubMed](#)]
25. Luzio, J.P.; Parkinson, M.D.J.; Gray, S.R.; Bright, N.A. The Delivery of Endocytosed Cargo to Lysosomes. *Biochem. Soc. Trans.* **2009**, *37*, 1019–1021. [[CrossRef](#)] [[PubMed](#)]
26. Feyder, S.; De Craene, J.-O.; Bär, S.; Bertazzi, D.; Friant, S. Membrane Trafficking in the Yeast *Saccharomyces cerevisiae* Model. *Int. J. Mol. Sci.* **2015**, *16*, 1509–1525. [[CrossRef](#)] [[PubMed](#)]
27. Ma, M.; Burd, C.G. Retrograde Trafficking and Plasma Membrane Recycling Pathways of the Budding Yeast *Saccharomyces cerevisiae*. *Traffic* **2020**, *21*, 45–59. [[CrossRef](#)] [[PubMed](#)]
28. O'Sullivan, M.J.; Lindsay, A.J. The Endosomal Recycling Pathway—At the Crossroads of the Cell. *Int. J. Mol. Sci.* **2020**, *21*, 6074. [[CrossRef](#)] [[PubMed](#)]
29. Bowers, K.; Stevens, T.H. Protein Transport from the Late Golgi to the Vacuole in the Yeast *Saccharomyces cerevisiae*. *Biochim. Biophys. Acta—Mol. Cell Res.* **2005**, *1744*, 438–454. [[CrossRef](#)]
30. Lynch-Day, M.A.; Klionsky, D.J. The Cvt Pathway as a Model for Selective Autophagy. *FEBS Lett.* **2010**, *584*, 1359–1366. [[CrossRef](#)]
31. Galaris, D.; Barbouti, A.; Pantopoulos, K. Iron Homeostasis and Oxidative Stress: An Intimate Relationship. *Biochim. Biophys. Acta—Mol. Cell Res.* **2019**, *1866*, 118535. [[CrossRef](#)] [[PubMed](#)]
32. Barbosa, A.D.; Osório, H.; Sims, K.J.; Almeida, T.; Alves, M.; Bielawski, J.; Amorim, M.A.; Moradas-Ferreira, P.; Hannun, Y.A.; Costa, V. Role for Sit4p-Dependent Mitochondrial Dysfunction in Mediating the Shortened Chronological Lifespan and Oxidative Stress Sensitivity of Isc1p-Deficient Cells. *Mol. Microbiol.* **2011**, *81*, 515–527. [[CrossRef](#)] [[PubMed](#)]
33. Teixeira, V.; Medeiros, T.C.; Vilaça, R.; Ferreira, J.; Moradas-Ferreira, P.; Costa, V. Ceramide Signaling Targets the PP2A-like Protein Phosphatase Sit4p to Impair Vacuolar Function, Vesicular Trafficking and Autophagy in Isc1p Deficient Cells. *Biochim. Biophys. Acta—Mol. Cell Biol. Lipids* **2016**, *1861*, 21–33. [[CrossRef](#)] [[PubMed](#)]
34. Pereira, C.; Pereira, A.T.; Osório, H.; Moradas-Ferreira, P.; Costa, V. Sit4p-Mediated Dephosphorylation of Atp2p Regulates ATP Synthase Activity and Mitochondrial Function. *Biochim. Biophys. Acta—Bioenergy* **2018**, *1859*, 591–601. [[CrossRef](#)] [[PubMed](#)]
35. Pereira, C.; Pereira, A.T.; Costa, V. Activation of SNF1/AMPK Mediates the Mitochondrial Derepression, Resistance to Oxidative Stress and Increased Lifespan of Cells Lacking the Phosphatase Sit4p. *Biochim. Biophys. Acta—Mol. Cell Res.* **2020**, *1867*, 118660. [[CrossRef](#)] [[PubMed](#)]
36. Bastians, H.; Ponstingl, H. The Novel Human Protein Serine/Threonine Phosphatase 6 Is a Functional Homologue of Budding Yeast Sit4p and Fission Yeast Ppe1, Which Are Involved in Cell Cycle Regulation. *J. Cell Sci.* **1996**, *109*, 2865–2874. [[CrossRef](#)] [[PubMed](#)]
37. Fernandez-Sarabia, M.J.; Sutton, A.; Zhong, T.; Arndt, K.T. SIT4 Protein Phosphatase Is Required for the Normal Accumulation of *SWI4*, *CLN1*, *CLN2*, and *HCS26* RNAs during Late G1. *Genes Dev.* **1992**, *6*, 2417–2428. [[CrossRef](#)] [[PubMed](#)]
38. Nickels, J.T.; Broach, J.R. A Ceramide-Activated Protein Phosphatase Mediates Ceramide-Induced G1 Arrest of *Saccharomyces cerevisiae*. *Genes Dev.* **1996**, *10*, 382–394. [[CrossRef](#)] [[PubMed](#)]
39. De La Torre-Ruiz, M.A.; Torres, J.; Ariño, J.; Herrero, E. Sit4 Is Required for Proper Modulation of the Biological Functions Mediated by Pkc1 and the Cell Integrity Pathway in *Saccharomyces cerevisiae*. *J. Biol. Chem.* **2002**, *277*, 33468–33476. [[CrossRef](#)]
40. Di Como, C.J.; Arndt, K.T. Nutrients, via the Tor Proteins, Stimulate the Association of Tap42 with Type 2A Phosphatases. *Genes Dev.* **1996**, *10*, 1904–1916. [[CrossRef](#)]
41. Zhang, W.; Du, G.; Zhou, J.; Chen, J. Regulation of Sensing, Transportation, and Catabolism of Nitrogen Sources in *Saccharomyces cerevisiae*. *Microbiol. Mol. Biol. Rev.* **2018**, *82*, e00040-17. [[CrossRef](#)] [[PubMed](#)]
42. Jablonka, W.; Guzmán, S.; Ramírez, J.; Montero-Lomelí, M. Deviation of Carbohydrate Metabolism by the SIT4 Phosphatase in *Saccharomyces cerevisiae*. *Biochim. Biophys. Acta—Gen. Subj.* **2006**, *1760*, 1281–1291. [[CrossRef](#)] [[PubMed](#)]
43. Bozaquel-Morais, B.L.; Madeira, J.B.; Maya-Monteiro, C.M.; Masuda, C.A.; Montero-Lomelí, M. A New Fluorescence-Based Method Identifies Protein Phosphatases Regulating Lipid Droplet Metabolism. *PLoS ONE* **2010**, *5*, e13692. [[CrossRef](#)] [[PubMed](#)]
44. Masuda, C.A.; Ramírez, J.; Peña, A.; Montero-Lomelí, M. Regulation of Monovalent Ion Homeostasis and pH by the Ser-Thr Protein Phosphatase SIT4 in *Saccharomyces cerevisiae*. *J. Biol. Chem.* **2000**, *275*, 30957–30961. [[CrossRef](#)] [[PubMed](#)]
45. Bhandari, D.; Zhang, J.; Menon, S.; Lord, C.; Chen, S.; Helm, J.R.; Thorsen, K.; Corbett, K.D.; Hay, J.C.; Ferro-Novick, S. Sit4p/PP6 Regulates ER-to-Golgi Traffic by Controlling the Dephosphorylation of COPII Coat Subunits. *Mol. Biol. Cell* **2013**, *24*, 2727–2738. [[CrossRef](#)] [[PubMed](#)]
46. Luke, M.M.; Della Seta, F.; Di Como, C.J.; Sugimoto, H.; Kobayashi, R.; Arndt, K.T. The SAPs, a New Family of Proteins, Associate and Function Positively with the SIT4 Phosphatase. *Mol. Cell. Biol.* **1996**, *16*, 2744–2755. [[CrossRef](#)] [[PubMed](#)]
47. Woodacre, A.; Lone, M.A.; Jablonowski, D.; Schneiter, R.; Giorgini, F.; Schaffrath, R. A Novel Sit4 Phosphatase Complex Is Involved in the Response to Ceramide Stress in Yeast. *Oxid. Med. Cell. Longev.* **2013**, *2013*, 129645. [[CrossRef](#)] [[PubMed](#)]

48. Tate, J.J.; Tolley, E.A.; Cooper, T.G. Sit4 and PP2A Dephosphorylate Nitrogen Catabolite Repression-Sensitive Gln3 When TorC1 Is up- as Well as Downregulated. *Genetics* **2019**, *212*, 1205–1225. [[CrossRef](#)] [[PubMed](#)]
49. Teixeira, V.; Medeiros, T.C.; Vilaça, R.; Pereira, A.T.; Chaves, S.R.; Côrte-Real, M.; Moradas-Ferreira, P.; Costa, V. Ceramide Signalling Impinges on Sit4p and Hog1p to Promote Mitochondrial Fission and Mitophagy in Isc1p-Deficient Cells. *Cell Signal.* **2015**, *27*, 1840–1849. [[CrossRef](#)]
50. Barbosa, A.D.; Graça, J.; Mendes, V.; Chaves, S.R.; Amorim, M.A.; Mendes, M.V.; Moradas-Ferreira, P.; Côrte-Real, M.; Costa, V. Activation of the Hog1p Kinase in Isc1p-Deficient Yeast Cells Is Associated with Mitochondrial Dysfunction, Oxidative Stress Sensitivity and Premature Aging. *Mech. Ageing Dev.* **2012**, *133*, 317–330. [[CrossRef](#)]
51. Gietz, R.D.; Schiestl, R.H. High-Efficiency Yeast Transformation Using the LiAc/SS Carrier DNA/PEG Method. *Nat. Protoc.* **2007**, *2*, 31–34. [[CrossRef](#)] [[PubMed](#)]
52. Wiederhold, E.; Gandhi, T.; Permentier, H.P.; Breitling, R.; Poolman, B.; Slotboom, D.J. The Yeast Vacuolar Membrane Proteome. *Mol. Cell Proteom.* **2009**, *8*, 380–392. [[CrossRef](#)] [[PubMed](#)]
53. Martins, T.S.; Costa, R.S.; Vilaça, R.; Lemos, C.; Teixeira, V.; Pereira, C.; Costa, V. Iron Limitation Restores Autophagy and Increases Lifespan in the Yeast Model of Niemann–Pick Type C1. *Int. J. Mol. Sci.* **2023**, *24*, 6221. [[CrossRef](#)] [[PubMed](#)]
54. Hughes, C.S.; Moggridge, S.; Müller, T.; Sorensen, P.H.; Morin, G.B.; Krijgsveld, J. Single-Pot, Solid-Phase-Enhanced Sample Preparation for Proteomics Experiments. *Nat. Protoc.* **2019**, *14*, 68–85. [[CrossRef](#)] [[PubMed](#)]
55. Osório, H.; Silva, C.; Ferreira, M.; Gullo, I.; Máximo, V.; Barros, R.; Mendonça, F.; Oliveira, C.; Carneiro, F. Proteomics Analysis of Gastric Cancer Patients with Diabetes Mellitus. *J. Clin. Med.* **2021**, *10*, 407. [[CrossRef](#)] [[PubMed](#)]
56. Fabrizio, P.; Longo, V.D. The Chronological Life Span of *Saccharomyces cerevisiae*. *Ageing Cell* **2003**, *2*, 73–81. [[CrossRef](#)] [[PubMed](#)]
57. Yang, R.; Chun, K.T.; Wek, R.C. Mitochondrial Respiratory Mutants in Yeast Inhibit Glycogen Accumulation by Blocking Activation of Glycogen Synthase. *J. Biol. Chem.* **1998**, *273*, 31337–31344. [[CrossRef](#)]
58. Golden, C.K.; Kazmirchuk, T.D.D.; McNally, E.K.; El Eissawi, M.; Gokbayrak, Z.D.; Richard, J.D.; Brett, C.L. A Two-Tiered System for Selective Receptor and Transporter Protein Degradation. *PLoS Genet.* **2022**, *18*, e1010446. [[CrossRef](#)]
59. Martins, T.S.; Pereira, C.; Canadell, D.; Vilaça, R.; Teixeira, V.; Moradas-Ferreira, P.; de Nadal, E.; Posas, F.; Costa, V. The Hog1p Kinase Regulates Aft1p Transcription Factor to Control Iron Accumulation. *Biochim. Biophys. Acta—Mol. Cell Biol. Lipids* **2018**, *1863*, 61–70. [[CrossRef](#)]
60. Vowinkel, J.; Hartl, J.; Butler, R.; Ralser, M. MitoLoc: A Method for the Simultaneous Quantification of Mitochondrial Network Morphology and Membrane Potential in Single Cells. *Mitochondrion* **2015**, *24*, 77–86. [[CrossRef](#)]
61. Westermann, B.; Neupert, W. Mitochondria-Targeted Green Fluorescent Proteins: Convenient Tools for the Study of Organelle Biogenesis in *Saccharomyces cerevisiae*. *Yeast* **2000**, *16*, 1421–1427. [[CrossRef](#)] [[PubMed](#)]
62. Pfaffl, M.W. A New Mathematical Model for Relative Quantification in Real-Time RT-PCR. *Nucleic Acids Res.* **2001**, *29*, e45. [[CrossRef](#)] [[PubMed](#)]
63. Li, J.; Hochstrasser, M. Selective Microautophagy of Proteasomes Is Initiated by ESCRT-0 and Is Promoted by Proteasome Ubiquitylation. *J. Cell Sci.* **2022**, *135*, jcs259393. [[CrossRef](#)] [[PubMed](#)]
64. Oku, M.; Maeda, Y.; Kagohashi, Y.; Kondo, T.; Yamada, M.; Fujimoto, T.; Sakai, Y. Evidence for ESCRT- and Clathrin-Dependent Microautophagy. *J. Cell Biol.* **2017**, *216*, 3263–3274. [[CrossRef](#)] [[PubMed](#)]
65. Bilodeau, P.S.; Urbanowski, J.L.; Winistorfer, S.C.; Piper, R.C. The Vps27p-Hse1p Complex Binds Ubiquitin and Mediates Endosomal Protein Sorting. *Nat. Cell Biol.* **2002**, *4*, 534–539. [[CrossRef](#)] [[PubMed](#)]
66. Katzmann, D.J.; Stefan, C.J.; Babst, M.; Emr, S.D. Vps27 Recruits ESCRT Machinery to Endosomes during MVB Sorting. *J. Cell Biol.* **2003**, *162*, 413–423. [[CrossRef](#)] [[PubMed](#)]
67. Marek, A.; Korona, R. Restricted Pleiotropy Facilitates Mutational Erosion of Major Life-History Traits. *Evolution* **2013**, *67*, 3077–3086. [[CrossRef](#)] [[PubMed](#)]
68. Cao, L.; Tang, Y.; Quan, Z.; Zhang, Z.; Oliver, S.G.; Zhang, N. Chronological Lifespan in Yeast Is Dependent on the Accumulation of Storage Carbohydrates Mediated by Yak1, Mck1 and Rim15 Kinases. *PLoS Genet.* **2016**, *12*, e1006458. [[CrossRef](#)]
69. Müller, M.; Schmidt, O.; Angelova, M.; Faserl, K.; Weys, S.; Kremser, L.; Pfaffenwimmer, T.; Dalik, T.; Kraft, C.; Trajanoski, Z.; et al. The Coordinated Action of the MVB Pathway and Autophagy Ensures Cell Survival during Starvation. *eLife* **2015**, *4*, e07736. [[CrossRef](#)]
70. Ebrahimi, M.; Habernig, L.; Broeskamp, F.; Aufschnaiter, A.; Diessl, J.; Atienza, I.; Matz, S.; Ruiz, F.A.; Büttner, S. Phosphate Restriction Promotes Longevity via Activation of Autophagy and the Multivesicular Body Pathway. *Cells* **2021**, *10*, 3161. [[CrossRef](#)]
71. Ivashov, V.; Zimmer, J.; Schwabl, S.; Kahlhofer, J.; Weys, S.; Gstir, R.; Jakschitz, T.; Kremser, L.; Bonn, G.K.; Lindner, H.; et al. Complementary A-Arrestin-Ubiquitin Ligase Complexes Control Nutrient Transporter Endocytosis in Response to Amino Acids. *eLife* **2020**, *9*, e58246. [[CrossRef](#)] [[PubMed](#)]
72. Hatakeyama, R.; De Virgilio, C. TORC1 Specifically Inhibits Microautophagy through ESCRT-0. *Curr. Genet.* **2019**, *65*, 1243–1249. [[CrossRef](#)] [[PubMed](#)]
73. Morshed, S.; Tasnin, M.N.; Ushimaru, T. ESCRT Machinery Plays a Role in Microautophagy in Yeast. *BMC Mol. Cell Biol.* **2020**, *21*, 70. [[CrossRef](#)] [[PubMed](#)]
74. Hatakeyama, R.; Péli-Gulli, M.P.; Hu, Z.; Jaquenoud, M.; Garcia Osuna, G.M.; Sardu, A.; Dengiel, J.; De Virgilio, C. Spatially Distinct Pools of TORC1 Balance Protein Homeostasis. *Mol. Cell* **2019**, *73*, 325–338.e8. [[CrossRef](#)]

75. Bonangelino, C.J.; Chavez, E.M.; Bonifacino, J.S. Genomic Screen for Vacuolar Protein Sorting Genes in *Saccharomyces cerevisiae*. *Mol. Biol. Cell* **2002**, *13*, 2486–2501. [[CrossRef](#)] [[PubMed](#)]
76. Piper, R.C.; Cooper, A.A.; Yang, H.; Stevens, T.H. VPS27 Controls Vacuolar and Endocytic Traffic through a Prevacuolar Compartment in *Saccharomyces cerevisiae*. *J. Cell Biol.* **1995**, *131*, 603–617. [[CrossRef](#)] [[PubMed](#)]
77. Raymond, C.K.; Howald-Stevenson, I.; Vater, C.A.; Stevens, T.H. Morphological Classification of the Yeast Vacuolar Protein Sorting Mutants: Evidence for a Prevacuolar Compartment in Class E Vps Mutants. *Mol. Biol. Cell* **1992**, *3*, 1389–1402. [[CrossRef](#)]
78. Liang, Y. Phagophore-Lysosome/Vacuole Fusion in Mutant Yeast and Mammalian Cells. *Autophagy* **2023**, *19*, 2595–2600. [[CrossRef](#)]
79. Sun, L.X.; Qian, H.; Liu, M.Y.; Wu, M.H.; Wei, Y.Y.; Zhu, X.M.; Lu, J.P.; Lin, F.C.; Liu, X.H. Endosomal Sorting Complexes Required for Transport-0 (ESCRT-0) Are Essential for Fungal Development, Pathogenicity, Autophagy and ER-Phagy in *Magnaporthe oryzae*. *Environ. Microbiol.* **2022**, *24*, 1076–1092. [[CrossRef](#)]
80. Hansen, M.; Rubinsztein, D.C.; Walker, D.W. Autophagy as a Promoter of Longevity: Insights from Model Organisms. *Nat. Rev. Mol. Cell Biol.* **2018**, *19*, 579–593. [[CrossRef](#)]
81. Nair, U.; Thumm, M.; Klionsky, D.J.; Krick, R. GFP-Atg8 Protease Protection as a Tool to Monitor Autophagosome Biogenesis. *Autophagy* **2011**, *7*, 1546–1550. [[CrossRef](#)] [[PubMed](#)]
82. Yorimitsu, T.; He, C.; Wang, K.; Klionsky, D.J. Tap42-Associated Protein Phosphatase Type 2A Negatively Regulates Induction of Autophagy. *Autophagy* **2009**, *5*, 616–624. [[CrossRef](#)] [[PubMed](#)]
83. Strohlic, T.I.; Schmiedekamp, B.C.; Lee, J.; Katzmann, D.J.; Burd, C.G. Opposing Activities of the Snx3-Retromer Complex and ESCRT Proteins Mediate Regulated Cargo Sorting at a Common Endosome. *Mol. Biol. Cell* **2008**, *19*, 4694–4706. [[CrossRef](#)] [[PubMed](#)]
84. Ahuatzzi, D.; Riera, A.; Peláez, R.; Herrero, P.; Moreno, F. Hxk2 Regulates the Phosphorylation State of Mig1 and Therefore Its Nucleocytoplasmic Distribution. *J. Biol. Chem.* **2007**, *282*, 4485–4493. [[CrossRef](#)] [[PubMed](#)]
85. Moreno, F.; Herrero, P. The Hexokinase 2-Dependent Glucose Signal Transduction Pathway of *Saccharomyces cerevisiae*. *FEMS Microbiol. Rev.* **2002**, *26*, 83–90. [[CrossRef](#)] [[PubMed](#)]
86. Barbosa, A.D.; Pereira, C.; Osório, H.; Moradas-Ferreira, P.; Costa, V. The Ceramide-Activated Protein Phosphatase Sit4p Controls Lifespan, Mitochondrial Function and Cell Cycle Progression by Regulating Hexokinase 2 Phosphorylation. *Cell Cycle* **2016**, *15*, 1620–1630. [[CrossRef](#)] [[PubMed](#)]
87. Jin, C.; Barrientos, A.; Epstein, C.B.; Butow, R.A.; Tzagoloff, A. SIT4 Regulation of Mig1p-Mediated Catabolite Repression in *Saccharomyces cerevisiae*. *FEBS Lett.* **2007**, *581*, 5658–5663. [[CrossRef](#)]
88. Ruiz, A.; Xu, X.; Carlson, M. Roles of Two Protein Phosphatases, Reg1-Glc7 and Sit4, and Glycogen Synthesis in Regulation of SNF1 Protein Kinase. *Proc. Natl. Acad. Sci. USA* **2011**, *108*, 6349–6354. [[CrossRef](#)] [[PubMed](#)]
89. Ruiz, A.; Liu, Y.; Xu, X.; Carlson, M. Heterotrimer-Independent Regulation of Activation-Loop Phosphorylation of Snf1 Protein Kinase Involves Two Protein Phosphatases. *Proc. Natl. Acad. Sci. USA* **2012**, *109*, 8652–8657. [[CrossRef](#)]
90. Treitel, M.A.; Kuchin, S.; Carlson, M. Snf1 Protein Kinase Regulates Phosphorylation of the Mig1 Repressor in *Saccharomyces cerevisiae*. *Mol. Cell. Biol.* **1998**, *18*, 6273–6280. [[CrossRef](#)]
91. Barros, M.H.; Bandy, B.; Tahara, E.B.; Kowaltowski, A.J. Higher Respiratory Activity Decreases Mitochondrial Reactive Oxygen Release and Increases Life Span in *Saccharomyces cerevisiae*. *J. Biol. Chem.* **2004**, *279*, 49883–49888. [[CrossRef](#)] [[PubMed](#)]
92. Pan, Y.; Schroeder, E.A.; Ocampo, A.; Barrientos, A.; Shadel, G.S. Regulation of Yeast Chronological Life Span by TORC1 via Adaptive Mitochondrial ROS Signaling. *Cell Metab.* **2011**, *13*, 668–678. [[CrossRef](#)] [[PubMed](#)]
93. Ng, M.Y.W.; Wai, T.; Simonsen, A. Quality Control of the Mitochondrion. *Dev. Cell* **2021**, *56*, 881–905. [[CrossRef](#)] [[PubMed](#)]
94. Guo, J.; Chiang, W. Mitophagy in Aging and Longevity. *IUBMB Life* **2022**, *74*, 296–316. [[CrossRef](#)] [[PubMed](#)]
95. Gottlieb, R.A.; Bernstein, D. Mitochondrial Remodeling: Rearranging, Recycling, and Reprogramming. *Cell Calcium* **2016**, *60*, 88–101. [[CrossRef](#)] [[PubMed](#)]
96. Innokentev, A.; Kanki, T. Mitophagy in Yeast: Molecular Mechanism and Regulation. *Cells* **2021**, *10*, 3569. [[CrossRef](#)]
97. Campbell, C.L.; Thorsness, P.E. Escape of Mitochondrial DNA to the Nucleus in Yme1 Yeast Is Mediated by Vacuolar-Dependent Turnover of Abnormal Mitochondrial Compartments. *J. Cell Sci.* **1998**, *111*, 2455–2464. [[CrossRef](#)]
98. Seo, A.Y.; Joseph, A.-M.; Dutta, D.; Hwang, J.C.Y.; Aris, J.P.; Leeuwenburgh, C. New Insights into the Role of Mitochondria in Aging: Mitochondrial Dynamics and More. *J. Cell Sci.* **2010**, *123*, 2533–2542. [[CrossRef](#)] [[PubMed](#)]
99. Madeo, F.; Zimmermann, A.; Maiuri, M.C.; Kroemer, G. Essential Role for Autophagy in Life Span Extension. *J. Clin. Investig.* **2015**, *125*, 85–93. [[CrossRef](#)]
100. Tang, F.; Watkins, J.W.; Bermudez, M.; Gray, R.; Gaban, A.; Portie, K.; Grace, S.; Kleve, M.; Craciun, G. A Life-Span Extending Form of Autophagy Employs the Vacuole-Vacuole Fusion Machinery. *Autophagy* **2008**, *4*, 874–886. [[CrossRef](#)]
101. Athané, A.; Buisson, A.; Challier, M.; Beaumatin, F.; Manon, S.; Bhatia-Kiššová, I.; Camougrand, N. Insights into the Relationship between the Proteasome and Autophagy in Human and Yeast Cells. *Int. J. Biochem. Cell Biol.* **2015**, *64*, 167–173. [[CrossRef](#)] [[PubMed](#)]
102. Nam, T.; Han, J.H.; Devkota, S.; Lee, H.-W. Emerging Paradigm of Crosstalk between Autophagy and the Ubiquitin-Proteasome System. *Mol. Cells* **2017**, *40*, 897–905. [[CrossRef](#)]
103. Ji, C.H.; Kwon, Y.T. Crosstalk and Interplay between the Ubiquitin-Proteasome System and Autophagy. *Mol. Cells* **2017**, *40*, 441–449. [[CrossRef](#)] [[PubMed](#)]
104. Dikic, I. Proteasomal and Autophagic Degradation Systems. *Annu. Rev. Biochem.* **2017**, *86*, 193–224. [[CrossRef](#)] [[PubMed](#)]

105. Singer, T.; Haefner, S.; Hoffmann, M.; Fischer, M.; Ilyina, J.; Hilt, W. Sit4 Phosphatase Is Functionally Linked to the Ubiquitin-Proteasome System. *Genetics* **2003**, *164*, 1305–1321. [[CrossRef](#)]
106. Perez-Riverol, Y.; Bai, J.; Bandla, C.; García-Seisdedos, D.; Hewapathirana, S.; Kamatchinathan, S.; Kundu, D.J.; Prakash, A.; Frericks-Zipper, A.; Eisenacher, M.; et al. The PRIDE Database Resources in 2022: A Hub for Mass Spectrometry-Based Proteomics Evidences. *Nucleic Acids Res.* **2022**, *50*, D543–D552. [[CrossRef](#)]

Disclaimer/Publisher’s Note: The statements, opinions and data contained in all publications are solely those of the individual author(s) and contributor(s) and not of MDPI and/or the editor(s). MDPI and/or the editor(s) disclaim responsibility for any injury to people or property resulting from any ideas, methods, instructions or products referred to in the content.